https://doi.org/10.5194/egusphere-2025-1421
Preprint. Discussion started: 3 April 2025

Overcoming Challenges in Coastal Marine Heatwave Detection: Integrating In Situ and Satellite Data in Complex Coastal Environment

Cécile Pujol[1], Alexander Barth[1], Iván Pérez-Santos[2,3,4], Pamela Muñoz-Linford[3], Aida Alvera-Azcárate[1]

[1]GeoHydrodynamics and Environment Research, University of Liège, Liège, 4000, Belgium
[2]Centro de investigación i~mar, Universidad de Los Lagos, Puerto Montt, Chile
[3]Centro de Investigación Oceanográfica en el Pacífico Sur-Oriental COPAS COASTAL, Departamento de Oceanografía, Universidad de Concepción, Chile
[4]Centro de Investigación en Ecosistemas de la Patagonia (CIEP), Coyhaique, Chile

Correspondence to: Cécile Pujol (cecile.pujol@uliege.be)

Abstract. Marine Heatwaves (MHWs) and Marine Cold Spells (MCSs) are extreme sea temperature events characterised respectively by unusually warm and cold conditions, that can persist from days to months. Both events occur in every ocean, but MHWs are becoming more frequent and intense due to global warming, to the detriment of MCSs. They are generally studied using satellite data with long temporal resolution to build a long-term climatology of the sea temperature. While MHWs and MCSs occurring in the open ocean have been well studied and documented, their occurrence and dynamics in coastal environment remain poorly understood, mainly due to the lack of data available. Indeed, coastal regions exhibit complex characteristics due to intricate coastal dynamics, the presence geographical features such as of gulfs, islands, channels or fjords, posing significant challenges for satellite observation.

In this study, we investigate the development and characteristics of MHWs and MCSs in Chilean Northern Patagonia over the period 2003-2023, as well as their seasonality and trends. Chilean Northern Patagonia is characterised by its complex geography, with the presence of thousands of islands, fjords, channels and gulfs. We present here a new methodology for MHWs and MCSs detection, using a combination of in situ and satellite data. Since the 1990s, Northern Patagonia has been well sampled, resulting in approximatively 3 million of samples across different depths. We interpolated these data using the DIVAnd algorithm to obtain a daily climatology of the sea temperature at 32 different depths (from the surface to 400m) with a spatial resolution of 900m that does resolve all the channels and fjords of the study area. Satellite data were used for threshold determination and to compare daily temperature to the climatology. The combination of the in situ-based dataset and the satellite-based do enable the detection of MHWs at very high resolution.

Our findings reveal that MHWs tend to be more frequent across most of the study area, whereas MCSs are becoming less common. MHWs and MCSs intensity is generally much higher in the most enclosed basins of the study area, with an average intensity of 2.5°C for MHWs and -1.5°C for MCSs in those places. However, MCSs intensity tends to increase over time whereas MHWs intensity tends to decrease in most basins. Some case studies are also described, including a succession of MCSs and MHWs in 2007-2008, and prolonged MHWs conditions during 2016-2017.

https://doi.org/10.5194/egusphere-2025-1421
Preprint. Discussion started: 3 April 2025

1 Introduction

Marine heatwaves (MHWs) and marine cold spells (MCSs) are phenomena characterized by anomalously warm or cold water events that persist for at least 5 days to several months, as defined by Hobday et al. (2016) and Schlegel et al. (2021). MHWs have been increasingly observed worldwide, with rising intensity and duration linked to global warming (Oliver et al., 2018; Laufkötter et al., 2020; Cheng et al., 2023; Capotondi et al., 2024), while MCSs, although much less studied, are generally declining (Yao et al., 2022).

MHWs are responsible for increasing ocean stratification (Holbrook et al., 2020), decreasing oxygen concentration (Brauko et al., 2020; Gruber et al., 2021; Shunk et al., 2024) and increasing ocean acidification (Gruber et al., 2021; Burger et al., 2022; Mignot et al., 2022). They are also responsible for numerous impacts on biodiversity (Smith et al., 2023), among others, coral bleaching (Dalton et al., 2020; Soares et al., 2023; Huang et al., 2024), habitat loss (Arafeh-Dalmau et al., 2019; Filbee-Dexter et al., 2020), mass mortality (Garrabou et al., 2022), and favouring conditions for harmful algal blooms proliferation (Kuroda et al., 2021; McCabe et al., 2016; Takagi et al., 2022), with economic repercussions on aquaculture, fisheries and tourism (Barbeaux et al., 2020; Cheung and Frölicher, 2020; Maulu et al., 2021; Smith et al., 2021). Similar observations can be made for MCSs (Schlegel et al., 2021).

MHWs and MCSs are identified by comparing daily sea temperature against a long-term climatology. Hobday et al. (2016) recommend to use at least 30 years of temperature data to study MHWs, as this duration captures decadal trends such as El Niño Southern Oscillation and includes periods that were less impacted by the global warming than present day. The 90th (10th) percentile typically marks MHWs (MCSs) threshold, though some studies adopt higher percentile to focus exclusively on the most extreme events, thereby excluding what might be considered as “normal” extreme events (e.g. Frölicher et al., 2018; Holbrook et al., 2019; Laufkötter et al., 2020).

The primary method for detecting and tracking MHWs and MCSs relies on global satellite products, notably NOAA’s Optimum Interpolation Sea Surface Temperature product (OISST; Huang et al., 2021), which has a resolution of 1/4°. This product has been popularly used to track MHWs at global, regional and basin scale all around the globe since the beginning of MHW research. Other studies are using models to investigate MHWs at both surface and subsurface (e.g. Guo et al., 2022; Wang et al., 2022; Pontoppidan et al., 2023), while studies based in in situ data remain scarce due to limited deployment of long-term monitoring equipment (e.g. Cook et al., 2022; Magel et al., 2022; Mazzini and Pianca, 2022).

Although MHWs in the open ocean have been well-documented, their occurrence and dynamics within coastal environments remain poorly understood. While global low and high-resolution sea surface temperature (SST) datasets derived from satellites have been used in coastal MHW research (e.g. Marin et al., 2021; Dabulevičienė and Servaitė, 2024; Xie et al., 2024), they might be suboptimal for highly complex areas such as semi or fully-enclosed seas, or seas that comport a lot of channels, gulfs, islands or fjords.

https://doi.org/10.5194/egusphere-2025-1421
Preprint. Discussion started: 3 April 2025

Indeed, although fjords are present in regions of the world where MHWs have been investigated, such as New Zealand (Shi et al., 2020), Norway (Bayoumy et al., 2022; Jordà-Molina et al., 2023), Canada (Jackson et al., 2018; Khangaonkar et al., 2021), Chile (Pujol et al., 2022) or the Kerguelen Islands (Su et al., 2021), very few studies have been conducted to understand how MHWs interact with fjords. It is largely due to the observational challenges these regions present, particularly for satellites which are compromised by land interferences and typically rainy and/or cloudy climate associated with fjords, which results in data loss. Nevertheless, a few studies have been conducted on MHWs in fjords using satellite data and models (Khangaonkar et al., 2021) and in situ data (Aksnes et al., 2019; Jackson et al., 2018, 2021; Jordà-Molina et al., 2023), providing insights on how fjord characteristics influence MHWs' dynamics. While precise data are unavailable, fjords ecosystems contribute significantly to the global aquaculture production, particularly Norwegian and Chilean fjord systems. MHWs could directly impact this production through thermal stress, and by favouring the development of fish-killing algae, or by increasing oxygen depletion (Díaz et al., 2023).

In this study, we are focusing on the Northern Patagonian Fjords, in southern Chile, with special interest on the Inner Sea of Chiloé (Fig. 1). This region is characterised by the presence of fjords, numerous islands and intricate channels, restricting the water exchanges with the Pacific Ocean and shielding the Inner Sea.

We propose a novel method for detecting MHWs and MCSs in coastal areas with complex features, which, to our knowledge, has never been used before, consisting in combining in situ and satellite data. We used in situ data to build a daily climatology and satellite data to set thresholds and provide daily SST. This approach allows the detection of MHWs with a resolution of 900m, effectively capturing all the fjords and narrow channels of Northern Patagonia. Finally, we described the MHWs and MCSs characteristics and trends observed for the period 2003-2023 and examined case studies using the method described in the following section.

2 Material and Method

2.1 Study area

The Northern Patagonian Fjords is located in the south of Chile and represents the northernmost part of Chilean Patagonia (41°-56° S). It spans from 41.4° S to 46.7°S and from 72°W to 74°W (Fig. 1). It is delimited to the east by the continent, to the north-west by the Island of Chiloé, and to the south-west by the Chonos Archipelago composed of more than a thousand islands and playing a crucial role in reducing the wind stress and mitigating the waves intensity before they reach the mainland (Pinilla et al., 2019). To the west of the sea, the continental shelf drops sharply, with depths increasing rapidly to over 2000 m due to the presence of the Peru-Chile Trench. The Northern Patagonian Fjords encompasses diverse basins, channels and fjords. From north to south, the key areas include the large semi-enclosed gulf Reloncaví Sound and the Reloncaví Fjord, which flows into the sound. To the south of Reloncaví Sound, lies the Ancud Gulf and the Corcovado Gulf, separated by the Desertores Islands, forming a natural barrier separating the deeper waters of the Reloncaví Sound and Ancud Gulf from the shallower Corcovado Gulf. Ancud and Corcovado Gulf are regions more influenced by oceanic waters entering through the

https://doi.org/10.5194/egusphere-2025-1421
Preprint. Discussion started: 3 April 2025

Guafo Mouth (Calvete and Sobarzo, 2011; Pérez-Santos et al., 2014; Linford et al., 2023), with some fjords extending eastward into the continent. South of the Corcovado Gulf, lies the narrow canal of Moraleda, which transitions into the Elefantes Channel, forming an extensive and complex network of channels and fjords (Soto-Riquelme et al., 2023; Linford et al., 2024). The bathymetry in the Northern Patagonian Fjords is very complex due to its numerous microbasins and islands. Although the bathymetry is mainly lower than 400m, certain microbasins can be exceptionally deep, reaching for example the Jacaf channel with 600m depth (Schneider et al., 2014; Pinilla et al., 2020).

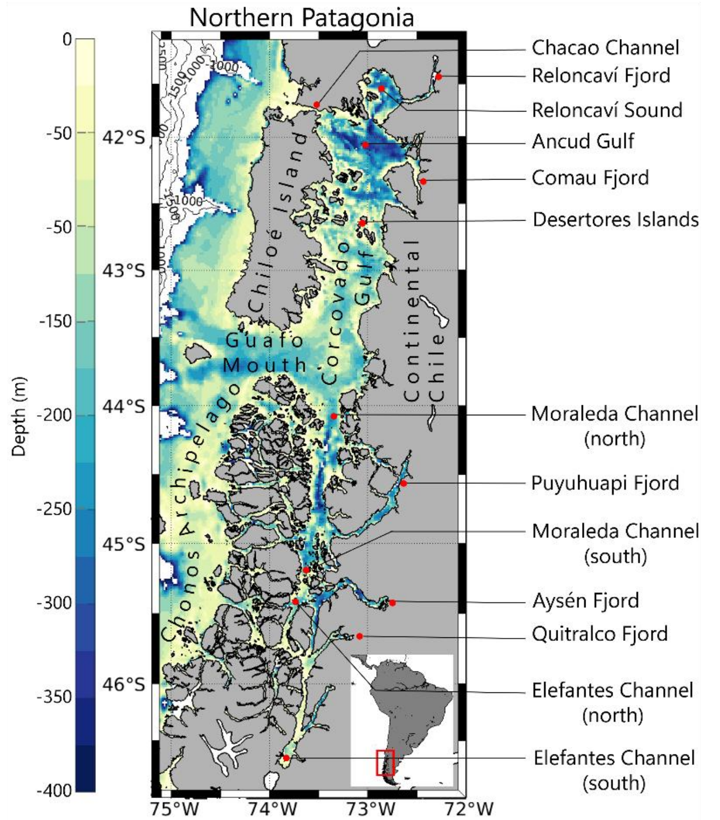

Figure 1: Map of the study area with depth. The level lines are indicating the depth every 500m.

2.2 Construction of a daily climatology with in situ data

To construct the climatology, we gathered all available in situ data to have the largest dataset possible. The data come from various online platforms and direct in situ measurements (see Supplementary Materials for details and DOIs of the in situ data). Only samples within the study area (-75.1°E, -72.0°E and -41.4°N, -46.7°N) were retained, encompassing both surface and depth. The entire dataset spans the period from 1948 to September 2022, although spatial and temporal coverage are sparse. Data selection involves using only valid flagged data when such indicators were available, and excluding "obviously" wrong data (such as temperatures superior to 30°C). Duplicates were eliminated if they met the following conditions: they were horizontally separated by less than 0.01° (about 1km), by less than 10 cm depth, sampled with no more than one day apart (considering that a significant part of the samples have a daily-precision and not a hourly one), and had a temperature differing by no more than +/- 0.1°C. In total, 3.3 million data samples were used for the climatology construction.

MHWs and MCSs detection requires a long-term climatology, typically based on at least 30 years of data, to compare with daily local SST (Hobday et al., 2016). This climatology is generally derived from long-term satellite data, with the NOAA OISST dataset (Huang et al., 2021) being the most commonly used (e.g. Hobday et al., 2016; Frölicher et al., 2018; Holbrook et al., 2019). However, long-term global satellite products often have a coarse resolution; for instance, the OISST product has a resolution of 1/4°. Unfortunately, the Northern Patagonian Fjords is not suitable for the use of long-term satellite data: it is

https://doi.org/10.5194/egusphere-2025-1421
Preprint. Discussion started: 3 April 2025

a quite narrow sea of fifty kilometres wide as a maximum, composed of various fjords and channels that cannot be adequately resolved by satellite data with a resolution of 1/4°. In addition, the weather in the study area is often rainy and cloudy (Garreaud and Aceituno, 2007), obscuring the view of the satellite sensors. Consequently, satellite data is not the preferred choice for this region. Fortunately, the Northern Patagonian Fjords has been extensively sampled over the last decades, resulting in a multitude of in situ data, totalling more than 3 million samples across all depths. We therefore decided to take benefits from the amount of in situ data to build the climatology.

Due to the sparse and discrete nature of the in situ data, it was necessary to interpolate these observations to create a continuous field. For this purpose, we employed DIVAnd (Data-Interpolating Variational Analysis in n dimensions), spatio-temporal interpolation tool for geophysical variables that utilises scattered, spatially and temporally irregularly distributed data to create a continuous field via variational interpolation, taking the bathymetry into account (Troupin et al., 2010; Barth et al., 2014). This tool is particularly well-suited for our study area since it can handle both spatial and temporal dimensions, allowing for the interpolation of data across 2D (longitude x latitude), 3D (time or depth) or 4D (time and depth). The input to provide is a field of potentially irregularly distributed data with associated coordinates (longitude and latitude) and date, and adjust specific parameters such as the expected error variance of the data, the resolution of the final grid or the smoothness of the interpolation. The variable to interpolate in this study was the temperature, with the objective to build a 4D climatology. First, a seasonal interpolation has been performed to create a seasonal climatology (January-February-March, April-May-June, July-August-September, October-November-December). This approach addresses the lack of in situ data in some areas of the sea and the absence of samplings during certain periods. Secondly, a second interpolation was realised to generate a monthly climatology. This involves repeating the earlier process using the same parameters but incorporating the seasonal climatology as a background, with the in situ data to refine the results into a monthly climatology. The final grid resolution was set at 0.008°, which corresponds approximately to 900m, covering the Northern Patagonian Fjords from -75,1°E to -72°E and -47°N to -41°N. Bathymetry data was sourced from the GEBCO dataset with a resolution of 30 seconds (https://www.gebco.net/data_and_products/gridded_bathymetry_data/). Temperature was interpolated over 32 different depth levels, irregularly distributed from the surface to a depth of 400m, with higher resolution at the surface (0m, 2.5m, 5m, 7.5m, 10m, 12.5m, 15m, 17.5m, 20m, 25m, 30m, 35m, 40m, 45m, 50m, 60m, 70m, 80m, 90m, 100m, 125m, 150m, 175m, 200m, 225m, 250m, 275m, 300m, 325m, 350m, 375m, 400m). The DIVAnd weight function was performed to reduce the influence of clustered data during the interpolation, with 0.1° (~10km) set as the threshold for identifying the clustered data. The interpolation smoothness was calibrated using a correlation length, defining the distance over which observations influence the interpolation, of 50 km horizontally and 50 m vertically and by setting an error variance of the observations that represents the level of confidence in the data multiplied by the weight attributed previously. The parameters were chosen to optimise metrics calculated for the validation of the climatology.

To validate the climatology, 5% of the data was put aside from the reconstruction process (see Appendix 1 for details on the in situ data used for validation). This data was subsequently used to conduct statistical tests and calculate different metrics

https://doi.org/10.5194/egusphere-2025-1421
Preprint. Discussion started: 3 April 2025

comparing the climatology to the data kept apart, including the correlation, the bias, the root mean square error (RMS), the centred root mean squared error (CRMS), and the standard deviation.

The DIVA interpolation results in a monthly climatology at 32 different depths with a resolution of approximately 900 m, effectively resolving all fjords and channels from the northern Patagonia. To overcome the monthly climatology and have a daily one, a 90-day moving average was calculated for each grid cell.

2.3 Calculation of a threshold

Thresholds for MHW (MCS) detection are based on the 90th (10th) percentile of the same temperature dataset used to construct the climatology (Hobday et al., 2016). However, we did not use satellite data for the climatology but relied instead on in situ data. While in situ data posed no issue for constructing the climatology, their limited availability in some places of the study area prevented the calculation of such kind of threshold. Some areas have been sparsely sampled or remain unsampled during some months of the year, making the determination of the 90th (10th) percentile from such sparse data meaningless.

We considered using a zonal threshold based on in situ data, i.e. pooling all the in situ data in one specific basin or fjord to define a single threshold for that area. However, this approach would have resulted in an insufficiently detailed representation of the dynamics of the sea.

Hence, we opted for satellite data for the surface threshold determination. Specifically, we used MODIS AQUA, providing sea surface temperature data (SST) with a daily temporal resolution from 2003 to June 2023 and a spatial resolution of 4 km, over the area -100°E to -70°E and -29°N to -55°N (https://podaac.jpl.nasa.gov/dataset/MODIS_AQUA_L3_SST_MID-IR_8DAY_4KM_NIGHTTIME_V2019.0#; NASA OBPG, 2020). However, this dataset is a level 3 product (L3) and contains gaps due to cloud cover, which is suboptimal for MHWs (MCSs) detection because it limits or prevents their tracking and their estimation of their spatial and temporal extensions which are criterions for their identification. Consequently, it was necessary to reconstruct the dataset to produce a gap-free field.

For this purpose, we used the interpolation tool DINEOF (Data INterpolating Empirical Orthogonal Functions) DINEOF aims to reconstruct spatial datasets by calculating empirical orthogonal functions (EOFs) to identify the dataset’s main patterns of variability. DINEOF is particularly relevant for satellite geophysical datasets that contain gaps due to cloud cover or precipitation (Alvera-Azcárate et al., 2005, 2011). To fill-in the missing data, DINEOF first removes a spatial and temporal mean from the original dataset, with missing data initially set to zero. Then, a first EOF decomposition is performed and the missing values are replaced with those estimated through the EOF decomposition. Some randomly chosen data is set aside and not used for the reconstruction to simultaneously calculate a cross-validation error. Then, the EOF decomposition and error calculation are repeated with 2 EOFs, then 3 EOFs, and so on, and the final number of EOFs retained corresponds to the minimal error obtained by the cross-validation. To optimise computation and avoid errors associated with handling large files, we applied DINEOF to the MODIS temperature dataset on a year-by-year basis.

After reconstructing the MODIS dataset, a horizontal bilinear interpolation was performed to match the spatial resolution and grid of the DIVA climatology. Once the satellite dataset was adapted (gap-filled and interpolated to match DIVA climatology’s grid), monthly averages were calculated to match the monthly climatology, and we extracted the 10th and 90th percentiles. As for the climatology calculation, a 90-day moving average was applied to ensure a smooth threshold. This process resulted in a daily threshold for each pixel of the study area, which could not have been feasible using only in situ data. The same dataset was used as daily SST for MHWs and MCSs detection.

To compare satellite data with the in situ climatology, we calculated the bias between the two datasets. Specifically, we calculated the difference between the monthly in situ climatology and the monthly satellite-derived threshold. This monthly difference was smoothed using a 90-days moving average to produce a daily bias correction, which was subtracted from the daily satellite dataset.

2.4 MHWs and MCSs detection

The detection of MHWs and MCSs is based on the comparison between daily climatology and daily temperature exceeding a threshold derived from the climatology (Hobday et al., 2016). Here, the climatology was calculated using in situ data, while the threshold and daily temperature were derived from satellite dataset, as explained in the previous section. The threshold corresponds respectively to the 90th and 10th percentile for MHWs and MCSs. Additionally, MHWs and MCSs were categorised following the definition of Hobday et al. (2018). It implies that category I event is encompassed between 1 and 2 times the difference between the climatology and the threshold, category II is between 2 and 3 times the difference, category III is between 3 and 4 times the difference, and category IV is superior to 4 times the difference. Different metrics were studied: the mean and maximal intensity of the different events (°C), their frequency (event/year), their duration (days), and cumulative intensity which corresponds to the sum of the temperature anomalies accumulated during the event (°C.day). The seasonality of MHWs and MCSs as well as their long-term trends were also analysed with those same metrics.

The detection process was realised using the m_mhw Matlab toolbox developed by Zhao and Marin (2019) following the definition of MHWs given by Hobday et al. (2016).

2.5 Atmospheric data

To understand atmospheric conditions before and during MHW/MCS events, we analysed different atmospheric parameters including the heat fluxes: the surface latent and sensible heat flux (respectively Qe and Qc), the net solar radiation that reaches the Earth surface (Qs), the surface net thermal radiation (Qb) which represents the difference between the downward and upward radiation received and emitted by the Earth’s surface. The total net heat flux (Qi) was calculated as the difference between the incoming solar radiation (Qs) and the other parameters (Qb, Qe, Qc). In other words, it represents the net solar radiation minus the heat reflected or lost by Earth’s surface, following Eq. (1) :

$$Qi = Qs - Qb - Qe - Qc$$

Additionally, we examined u and v wind components at 10m, atmospheric temperature at 2m, surface pressure, low and total cloud cover, total precipitation and evaporation. Those parameters were taken from ERA5 reanalysis data provided by the European Centre for Medium-Range Weather Forecast (ECMWF, Hersbach et al., 2023), available at

https://doi.org/10.5194/egusphere-2025-1421
Preprint. Discussion started: 3 April 2025

https://cds.climate.copernicus.eu/cdsapp#!/dataset/reanalysis-era5-single-levels?tab=form. This data has an hourly resolution and a spatial resolution of 1/4°. Data was downloaded over the region between 30°S to 55°S and 65°W to 90°W, spanning the years 2003 to 2023. Since the ERA dataset has an hourly resolution, a daily average was calculated to match with the climatology that also has a daily resolution. The anomaly of every parameter was calculated by subtracting the daily values from a climatology realised with the 20-years data.

3 Results and discussion

3.1 Validation of the climatology

To validate the climatology, 5% of the total in situ data was set aside and excluded from the reconstruction process (see Methods and Appendix). This reserved data was then used to compare with the climatology, and statistical analysis was performed. The root mean square error (RMSE) is the lowest during the winter months (May to September), which coincides with the months of lower standard deviation (Table 1). Overall, the RMSE and bias are quite low, while the correlation is notably high, indicating that the climatology is very close to the in situ observations. Since the RMSE is based on the difference between the climatology and instantaneous measurements, it also includes the sub-seasonal variability and interannual variability. Even a perfect climatology derived from an unlimited number of observations would not achieve zero RMS error and a perfect correlation of one. January and April exhibit the lowest correlations, which aligns with these months having the least available data. On average, 485 samples (not coming from moorings) are available per month, however, for January and April, only 99 and 161 are available respectively. The climatology is available on https://doi.org/10.5281/zenodo.14845077.

Table 1: Statistic metrics for the validation of the climatology at the surface level only (between 0 and 1m) for every month: Correlation, Bias (°C), Root mean square error (RMSE, °C), Centred root mean square error (CRMS, °C), the average Standard deviation (SD, °C) across the entire study area for the climatology, the average Standard deviation (°C) across the entire study area for the entire in situ dataset.

Month	Correlation	Bias (°C)	RMSE (°C)	CRMS (°C)	SD climatology	SD in situ data
Jan	0,159	0,214	1,847	1,834	1,160	1,974
Feb	0,709	0,039	1,433	1,433	1,274	2,054
Mar	0,320	0,112	1,141	1,135	1,019	1,685
Apr	0,171	-0,068	1,006	1,004	0,910	0,830
May	0,558	-0,082	0,783	0,779	0,937	0,774
Jun	0,810	-0,083	0,709	0,705	1,002	0,458
Jul	0,806	0,062	0,872	0,870	0,811	0,594
Aug	0,821	-0,139	0,707	0,693	0,536	0,580
Sep	0,748	0,010	0,731	0,731	0,608	0,511
Oct	0,396	0,202	0,952	0,930	0,672	0,817

Nov	0,410	0,086	1,232	1,229	0,738	1,234
Dec	0,446	0,105	1,421	1,417	1,081	2,184

3.2 Climatology

By processing the in situ data with DIVA, we produced a monthly climatology at 32 different depths from the surface to 400m (Fig. 2, 3, 4). At the surface (Fig. 2), summer months (Jan-Feb-Mar) are characterised by a strong west-east gradient in the open Pacific and another strong gradient in the Northern Patagonia, in Reloncaví Sound and Ancud Gulf. The other parts of the study area record temperatures between 12°C and 14°C, with maximums in February of about 18°C in Puyuhuapi Fjord, 17°C in Reloncaví Sound and Fjord, 16°C in Comau Fjord, (also observed by Castillo et al., 2016; León-Muñoz et al., 2013; Saldías et al., 2021; Linford et al., 2024) and in the north-western part of the domain in the open Pacific. Although located only 50 km south of Puyuhuapi Fjord, Aysén Fjord only reaches 13°C in February, possibly linked to a higher input of freshwater from the Andean melting in Aysén than in Puyuhuapi Fjord (Pinilla et al., 2019).

The Chacao Channel and south of Desertores Islands stand out as particularly cold regions, especially in February, also highlighted in the study Narváez et al. (2019). This same study suggested that the differences in temperature amplitudes in the Inner Sea of Chiloé might be linked to different influences of tides, water time residences and winds. During autumn (Apr-May-Jun), the climatology shows a general decline in temperatures, although a gradient persists in the northwest of the domain

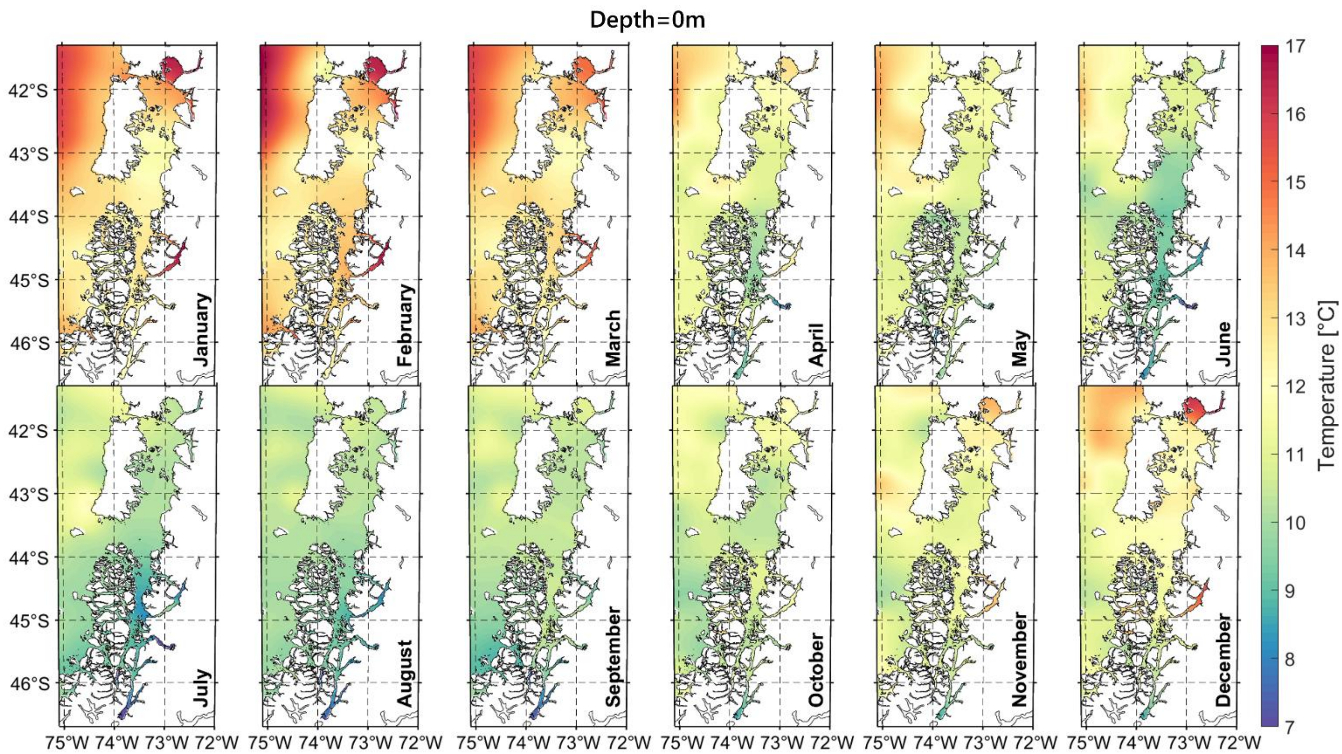

Figure 2: Monthly climatology of the sea temperature at the surface.

but much less intense than in summer. In June, a North-South temperature gradient in the study area appears, with values between 10°C and 11°C in Reloncaví Sound and 8°C at the extreme south (Fig. 2; Saldías et al., 2021; Linford et al., 2024). In winter (Jul-Aug-Sep), the surface temperatures are relatively uniform and show little variation. The temperature is the lowest in Elefantes Channel and Aysén Fjord, reaching 7°C, while most areas remain around 10°C. Notable exceptions include the slightly cooler Puyuhuapi Fjord and a potential warm anomaly southwest of Chiloé in July, possibly due to an anomalously warm measurement and inhomogeneous sampling in time.

The temperature in October is very similar to September, slightly warmer, reaching around 12°C in the north and in Puyuhuapi Fjord. Spring (Oct-Nov-Dec) sees gradual warming, with pre-summer conditions in December: 15°C to 17°C in Puyuhuapi Fjord and Reloncaví Sound, and the progressive development of a gradient in the open ocean. However, relatively cold temperatures are still present in the southern parts of the Northern Patagonia and west of Chonos Archipelagos, with overall temperatures below 11°C, and even dropping to 9°C in Elefantes Channel.

The surface climatology aligns with Saldías et al. (2021), who observed similar seasonal patterns from 2003-2019 satellite data: a strong gradient in summer in both the open ocean and the Northern Patagonian Fjord progressively fading away in autumn, a relatively homogeneous pattern in winter between 9°C and 12°C, and warming in spring.

Temperature fluctuations are more pronounced in enclosed areas: Reloncaví Sound varies from 10°C in winter to 17°C in summer, Puyuhuapi Fjord's head has a temperature that falls to 8°C in winter and rises to 18°C in summer, while in its central

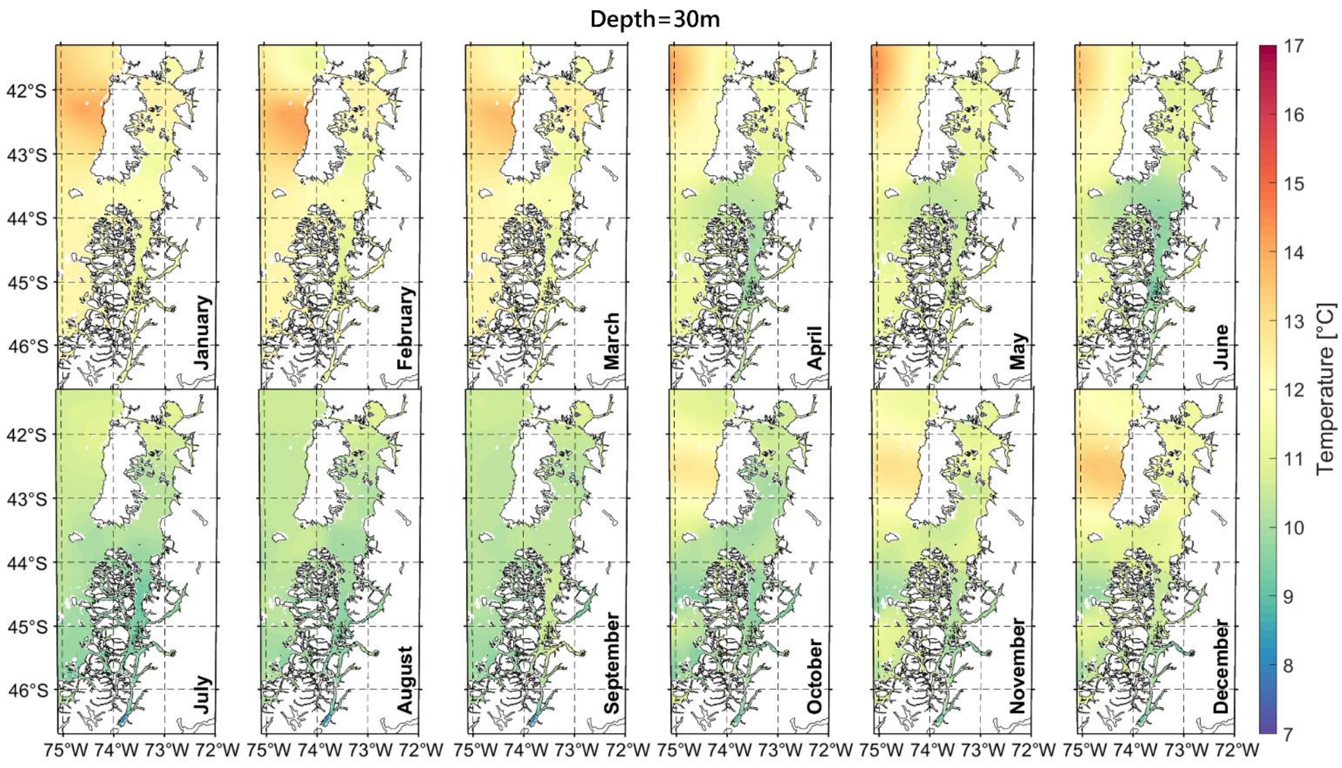

Figure 3: Monthly climatology of the sea temperature at 30m depth.

https://doi.org/10.5194/egusphere-2025-1421
Preprint. Discussion started: 3 April 2025

region it varies between 9°C and 16°C, coherent with Schneider et al. (2014), Pinilla et al. (2020) and Pérez-Santos et al. (2021)'s results. Aysén fjord shows a seasonal range between 6°C and 13°C at its head and between 9°C and 13°C at its mouth. In contrast, open areas experience slighter variations. Corcovado Gulf varies little throughout the year, ranging from 10°C in winter to 13°C in summer, as also reported by Buchan et al. (2021), Moraleda Channel vary from 9°C in winter to 13°C in summer, while Ancud Gulf varies from 11°C to 14°C. An exception is the open Pacific west of Chiloé, where temperatures vary significantly from 10°C to 17°C. However, West of Chonos Archipelago, variations are more modest, between 9°C and 13°C. Narváez et al. (2019) suggested that the greater warming in the northern half of the Northern Patagonia could be due to the Desertores Islands, which reduce winds and current velocities, allowing a greater warming of the sea surface.

Below the surface, the temperature decreases as expected and spatial temperature gradients are smoother, particularly in summer. For instance, at 30m depth, temperatures are almost homogeneous in winter (as observed in Pérez-Santos et al., 2021), while in summer they varie from 14°C west of Chiloé to 10°C in the southern part of the study area (Fig. 3).

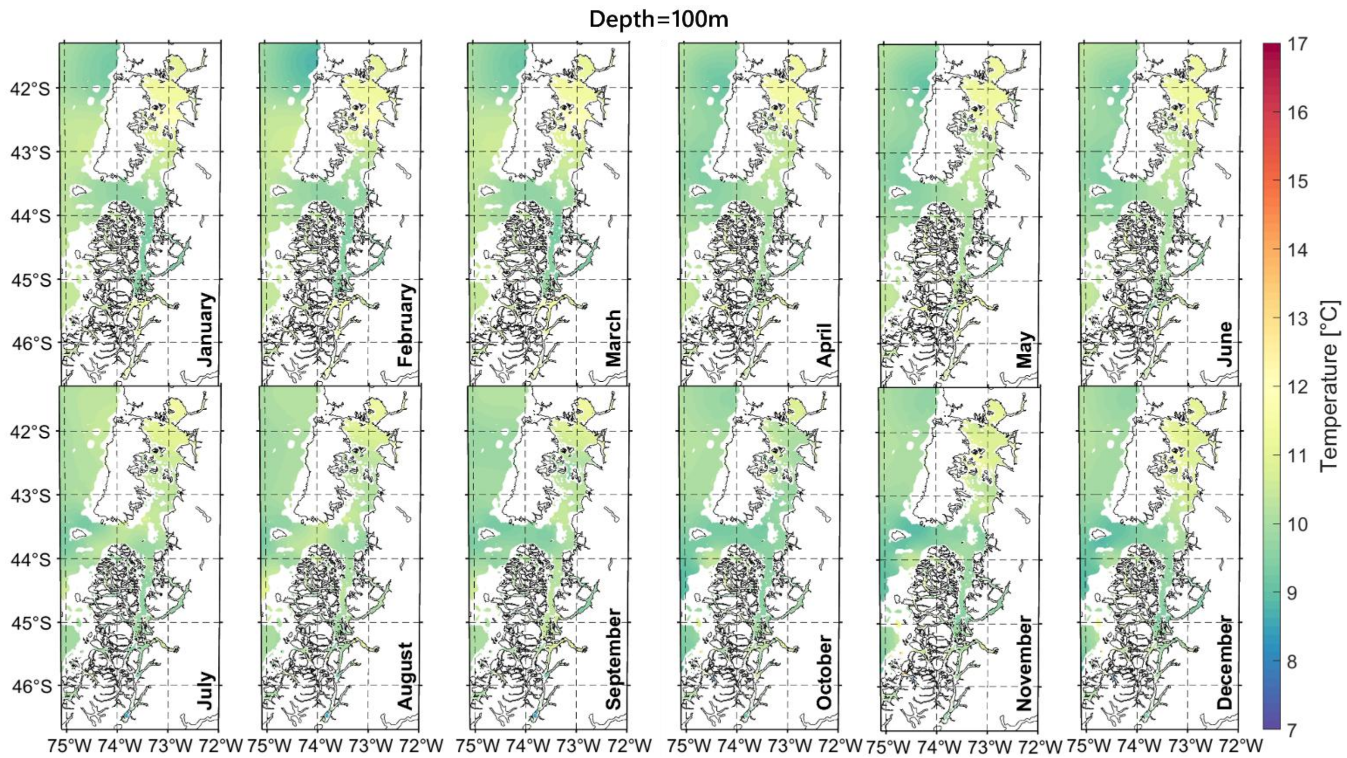

Figure 4: Monthly climatology of the sea temperature at 100m depth.

When reaching 100m depth (Fig. 4), temperature patterns remain consistent year-round, at round 10°C, aligning with Pinilla et al. (2021). Ancud Gulf, Reloncaví Sound and their associated fjords remain, slightly warmer with temperatures of 11°C in winter and 12°C in summer. At 200 meters depth, all year long, the temperature remains warmer in Ancud Gulf and Reloncaví Sound (10 to 11°C) than elsewhere (8 to 9°C), likely due to the Desertores Islands acting like a barrier, trapping warmer waters to the north (Pérez-Santos et al., 2021; Linford et al., 2024). At 400m depth, temperatures stabilise around 7°C in the entire study area and all year long, except in Aysén Fjord, where they fluctuate between 10°C (July to December) and 8.5°C (January-June). This particularity, consistent with the in situ samples that have been conducted over different years, may be linked to Aysén Fjord's long water residency time (120 days, Linford et al., 2024) inducing slower temperature changes.

In most basins, the thermocline typically lies between surface and 20 meters, strengthening in summer, as observed for instance in the Reloncaví Sound (Fig. 5A). However, the thermocline can extend deeper (up to 50m) as seen for instance west of Chiloé Island during summer, or in Aysén and Puyuhuapi Fjords (Fig. 5D). In Guafo Mouth and Corcovado Gulf, the thermocline can extend even further, ranging from 10 to 100m (Fig. 5C), reflecting the region's well-mixed nature (Calvete and Sobarzo, 2011). In winter, the entire water column is homogeneous, particularly around Chacao Channel, the northern half of Corcovado Gulf, and Ancud Gulf regions (Fig. 5B). The surface mixed layer is shallow in summer, usually under 10m, with strong surface stratification in fjords and enclosed basins (Fig. 5A and 5D), similar to observations in Finnish (Merkouriadi and Leppäranta, 2015) and Norwegian fjords (Skogseth et al., 2020). In the fjords, the stratification is higher at their heads than at their mouths, as regularly observed in other fjords, such as in south Patagonian fjords (e.g. Maturana-Martínez et al., 2021) or in Arctic fjords (e.g. Szeligowska et al., 2020).

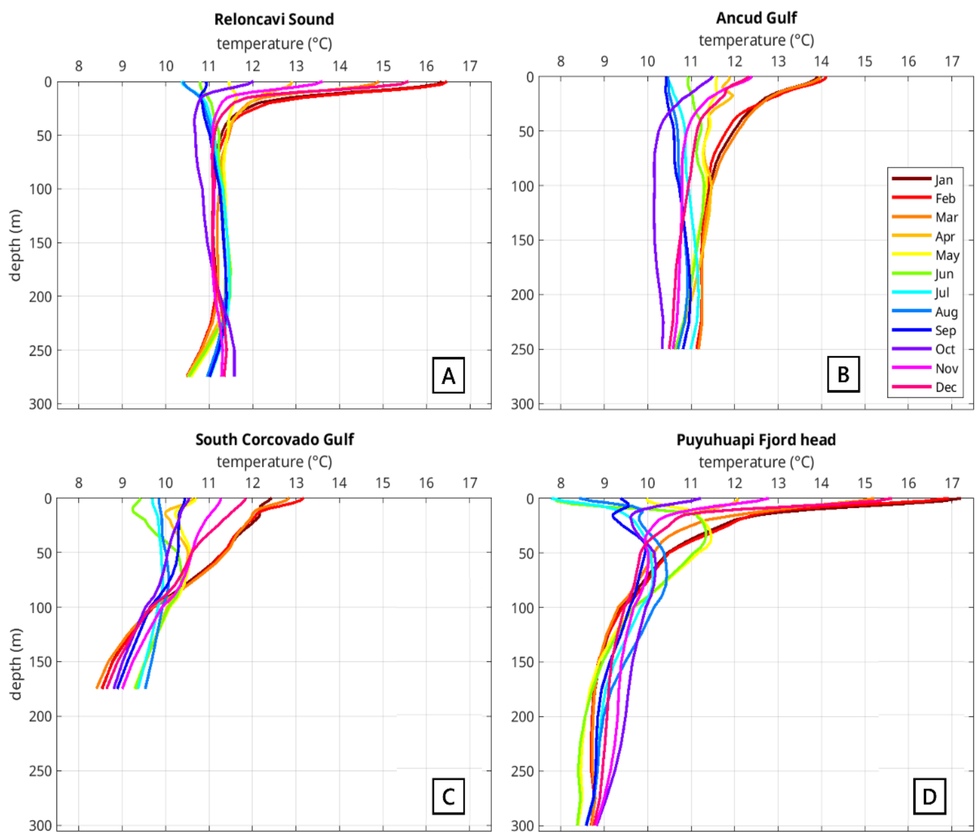

Figure 5: Profile plots of the climatology in different basins of the study area: A: Reloncaví Sound, B: Ancud Gulf, C: South of the Corcovado Gulf, D: the head of Puyuhuapi Fjord. Each colour represents the climatology for a specific month of the year. The profile terminates according to the local bathymetry.

3.3 Thresholds

The thresholds for detecting MHWs and MCSs (respectively the 90th and 10th percentile) were calculated using satellite data and by applying a temporal moving average to smooth it (see Methods). This approach ensures a consistent and coherent threshold for every place in the study area.

https://doi.org/10.5194/egusphere-2025-1421
Preprint. Discussion started: 3 April 2025

The results show that for every location, there is a difference of the thresholds' amplitude between summer and winter. While this difference is about a few decimals of a degree in most of the basins, the most pronounced variations are observed in the Reloncaví Sound with a threshold about 1.6°C above (below, for the 10th percentile) the climatology in summer and 0.6°C in winter. Similarly, in the Puyuhuapi Fjord, the thresholds are 1.9°C above (below) the climatology in summer and 0.8°C in winter. It can be noted that the locations with the highest threshold amplitudes also show the highest seasonal temperature amplitude. For the northern half of the domain, the high temperature amplitude has also been shown in Narváez et al. (2019) and Saldías et al. (2021).

3.4 DINEOF

To detect MHWs/MCSs, we used daytime L3 level satellite SST data from MODIS AQUA. However, this kind of data contains gaps due to cloud coverage or land contamination. It was therefore necessary to fill these gaps to enable the tracking of MHWs and MCSs. For this purpose, DINEOF was applied (see Methods) across a large area, from 29°S to 55°S and -100°W to -70°E.

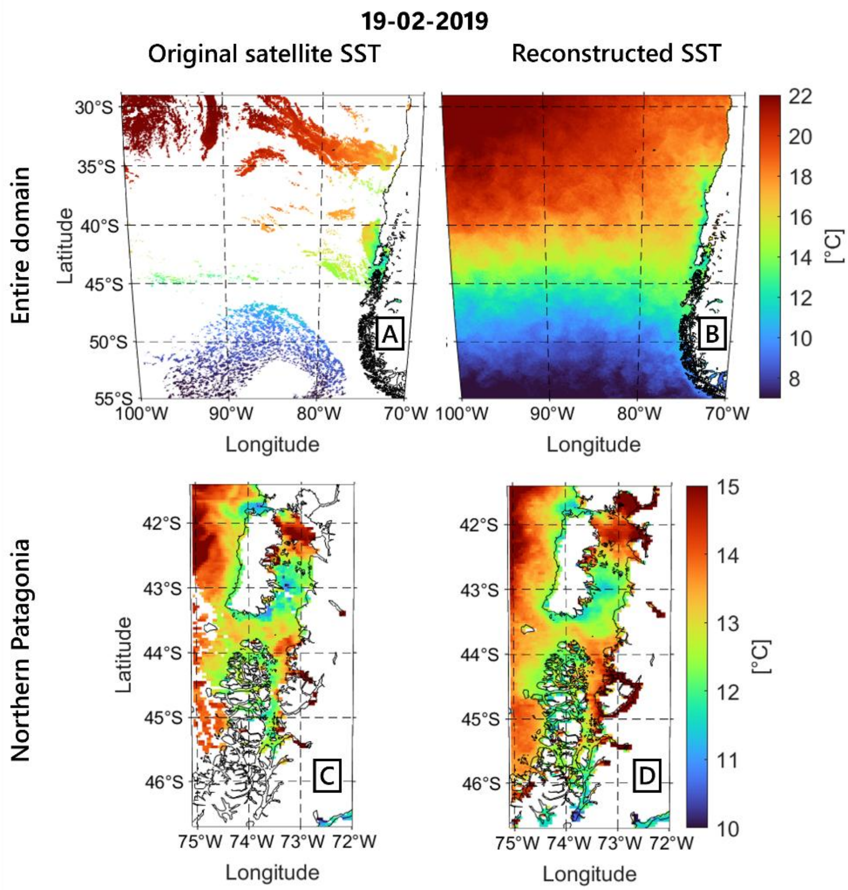

Figure 6: MODIS-AQUA satellite data (A,C) on the 7th of February 2019, and its reconstruction with DINEOF (B,D) over the entire domain (up) and with a zoom on the Inner Sea of Chiloé (bottom).

The reconstruction with DINEOF was conducted year by year from 2003 to 2023. Overall, over the entire domain, 78% of the data is missing. An example of the reconstruction is shown in Fig. 6.

DINEOF determines the optimal number of EOFs for each year using cross-validation, with an upper limit of 50 (see Fig. 7 for a typical year). On average, for each individual year from 2003 to 2023, 10 EOFs were selected as optimal. Typically, the first EOF represents 85.1% of the explained variance, the second one 14% and the third one 0.3%. Since we conducted the analysis year by year, we choose here to show the year 2019 which is representative of the other years. The first EOF, representing 84.7% of the explained variance, reveals a north-south gradient at about 40°S, likely due to the different atmospheric systems: a permanent anticyclone system along the coast of North Chile, and a cyclonic-dominated system to the south (Aguirre et al., 2012; Ancapichún and Garcés-Vargas, 2015). The second EOF (15% of the explained variance) shows a uniform pattern that switches state every year between the end of May and the beginning of June and between the end of November and the beginning of December. This EOF is probably associated with seasonal changes. The third EOF (0.3% of

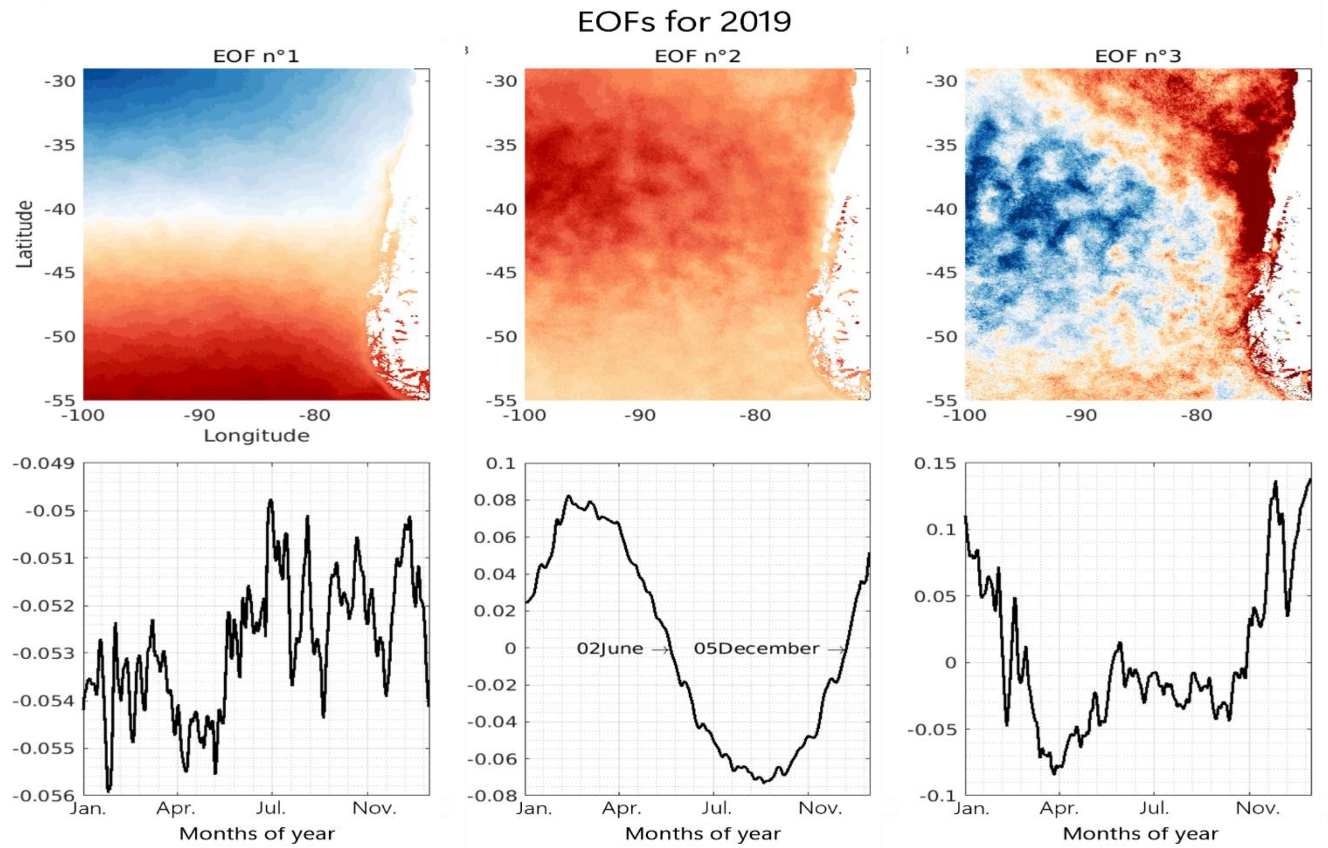

Figure 7: First 3 EOFs for the year 2019. Top: spatial EOF, Bottom: temporal variation. For the second EOF, there is a state switch that happens on the 2nd of June and on the 5th of December.

the explained variance) exhibits more small-scale variations and changes from year to year. However, a spatial pattern can be observed, with a coastal pattern present almost every year and an oceanic patch dissociated from the coastal pattern. No more than 3 EOFs were described as they represent for every year more than 99.4% of the total variance of the SST.

3.5 MHWs and MCSs from 2003 to 2023

The highest frequency of MHWs (Fig. 8A) can be found outside of the Northern Patagonian Fjords with an average of more than 2 events per year, as well as in the south of Corcovado Gulf, Guafo Mouth, Moraleda Channel, and the west part of Ancud Gulf and Comau Fjord. Conversely, the lowest frequencies are found south of Desertores Islands, offshore Chonos Archipelago and in Elefantes Channel. Considering the MCSs, Ancud Gulf and Reloncaví Sound stand out with an observed average frequency exceeding 2.5 events per year (Fig. 8E). In the South and West coast of Corcovado Gulf and in Moraleda Channel, the frequency is about 2 to 2.5 events a year, as well as along the west coast of Chiloé. Offshore Chiloé and on the west side

https://doi.org/10.5194/egusphere-2025-1421
Preprint. Discussion started: 3 April 2025

of Corcovado Gulf, the frequency of MCSs drops below 1.5 events per year. For both MHWs and MCSs, every single part of the study area experiences at least 1 event per year. MHW have been studied over a much larger area in Pujol 2022), showing an average of 1.8 events per year occurring between the 1980s and the 2020s, which is coherent with what was found here.

https://doi.org/10.5194/egusphere-2025-1421
Preprint. Discussion started: 3 April 2025

The mean intensity over the last 20 years is basin dependency (Fig. 8B): the highest intensities can be seen in the most enclosed areas: Reloncaví Sound with a mean intensity of 2°C (with a west-east gradient), in Aysén Fjord with a higher intensity at its

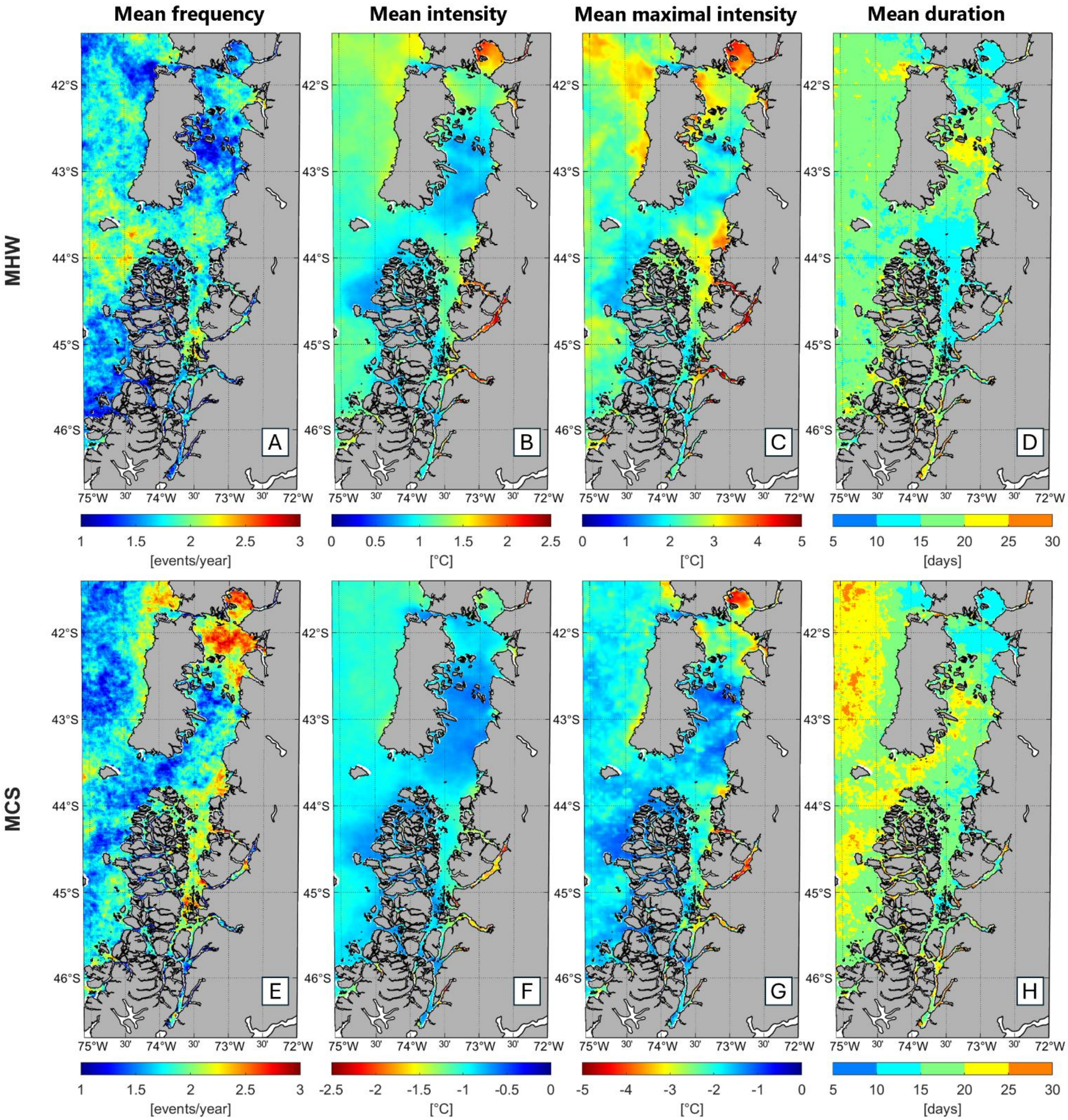

Figure 8: Spatial representation of the average Frequency (A, E), Mean Intensity (B, F), Mean Maximal Intensity (C, G), Duration (D, H) for MHW (top) and MCS (bottom) on the period 2003-2023.

https://doi.org/10.5194/egusphere-2025-1421
Preprint. Discussion started: 3 April 2025

head (more than 2°C), and the highest intensity is found in Puyuhuapi Fjord with an average intensity of 2.5°C in its centre (these regions correspond to the places with the highest seasonal temperature amplitude). A coastal zone along the western coast of Chiloé, excluding Chacao Channel, is also highlighted. In contrast, the lowest intensities are found in Corcovado Gulf and in the Chonos Archipelago, with values below 0.5°C, aligning with the regions with the lowest temperature amplitude. Examining the average maximum intensity of MHWs, similar patterns emerge (Fig. 8C): maximum intensities are found in enclosed areas, reaching up to 5°C in Aysén and Puyuhuapi Fjords and 4°C in Reloncaví Sound. The lowest maximal intensities, below 2°C, occur in Corcovado Gulf and Chonos Archipelago. Within the fjords, the intensity is generally higher in the most enclosed regions and diminishes towards their mouths. When looking at the MCSs (Fig. 8F), the intensity patterns are comparable. Intensities remain relatively mild in the Inner Sea of Chiloé and Chonos Archipelago (above -1°C), and stronger in the Reloncaví Sound (between -1.5°C and -1 °C), Comau, Puyuhuapi and Aysén Fjords (about -1.5°C and reaching -2.5°C at Puyuhuapi's head). For the maximum intensity (Fig. 8G), again, a similar pattern can be observed as for MHWs with a maximum intensity peaking at -5°C in Puyuhuapi Fjord and Reloncaví Sound, while most of the other parts of the study area experience maximum intensities above -2°C.

Regarding duration (Fig. 8D), the area around Desertores Islands is particularly impacted, with a mean duration between 20 and 25 days. The extreme South of the Inner Sea of Chiloé, the Elefantes channel and some channels of the Western part of Chonos Archipelago, also experience prolonged MHWs. Notably, the northwest of Chiloé Island is similarly affected. In the open-ocean, MHWs typically last over 15 days, whereas shorter durations, under 15 days, are recorded in south Corcovado Gulf, Moraleda Channel, Comau Fjord and Reloncaví Gulf.

For the MCSs, a clear distinction is visible between the open ocean and coastal environments: the average duration reaches 30 days in the open ocean, but decreases to less than 20 days along Chiloé shores (Fig. 8H). Within the Inner Sea of Chiloé, MCS length is generally shorter than 20 days, with the lowest length being in Reloncaví Sound and Ancud Gulf (between 10 and 15 days). However, along Chiloé's east coast, from Desertores Islands to further south, MCS lengths are significantly higher, averaging around 25 days. That pattern matches the overall circulation inside of the sea, with surface waters entering by the Boca del Guafo and following along the East coast of Chiloé up to Desertores Islands (Linford et al., 2023, 2024). On the other hand, upwelling intensification in the adjacent oceanic water to the west coast of Chiloé and Guafo Mouth could contribute to the MCS's duration (Aguirre et al., 2019; Narváez et al., 2019; Pérez-Santos et al., 2019).

Examining cumulative intensity (not shown), the Inner Sea of Chiloé and the southern part of the study area record relatively low averages, below 20°C.day, except for Puyuhuapi Fjord which reaches up to 50°C.day. West of Chiloé, cumulative intensities are slightly higher, ranging between 20 and 30°C.day. For MCSs, a similar pattern is observed, with higher values in the open ocean and Puyuhuapi and Aysén Fjords (-30 to -20°C.day) and lower values in the Inner Sea and Chonos Archipelago (-15 to -10°C.day).

https://doi.org/10.5194/egusphere-2025-1421
Preprint. Discussion started: 3 April 2025

3.6 MHWs and MCSs seasonality

The seasonality of MHWs and MCSs is highly evident. Indeed, on average, during summer, there are at least 3 days of MHWs per month in the period 2003-2023, up to 5 days in the East of Ancud and South of Corcovado Gulfs and up to 6 days in Moraleda Channel (Fig. 9B). In the open ocean, occurrences can reach up to 7 days per month. In winter, almost no MHWs are registered (fewer than 1 day per month; Fig 9D). Spring (Fig 7A) and autumn (Fig. 9C) lie in between, although in autumn MHWs are above all present in the open ocean, up to 4 days per month around Chiloé Island. Conversely, MCSs are far more frequent during winter (Fig. 9H), with a minimal occurrence of 3 days per month, and up to 6 days per month in Ancud Gulf

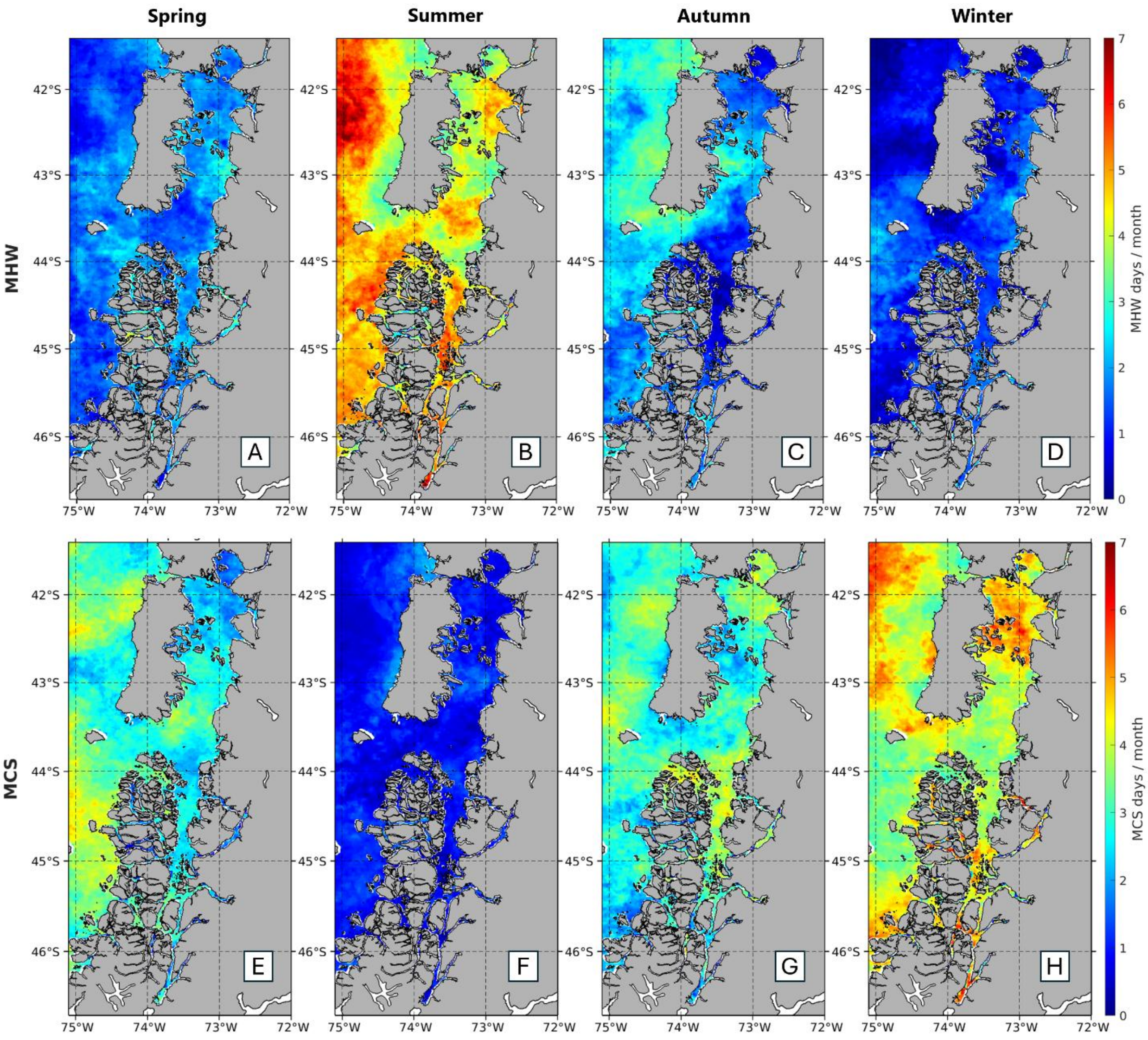

Figure 9: Seasonal occurrence of MHWs (top) and MCSs (bottom): Spring (A, E), Summer (B, F), Autumn (C, G), Winter (D, H). It represents the number of days under MHW/MCS condition per month for each season. Representation for the period 2003-2023.

https://doi.org/10.5194/egusphere-2025-1421
Preprint. Discussion started: 3 April 2025

and the open ocean. In summer, less than 1 event per month is registered (Fig. 9F). However, MCSs tend to occur more often during spring and autumn than MHWs, occurring more frequently outside of the Inner Sea in spring (Fig. 9E) and inside in autumn (Fig. 9G). The preferred occurrence of MHWs in summer and MCSs in winter is well known in literature and follows here what is commonly observed (Schlegel et al., 2021; Wang and Zhou, 2024).

When looking at the seasonal intensity of MHWs and MCSs, the patterns and intensities are remarkably similar. Indeed, in both cases, the least intense events are occurring in winter, with MCSs exhibiting a uniform distribution (Fig. 10H), and MHWs being slightly more intense in the open ocean than in the Northern Patagonian Fjords (Fig. 10D). However, in both cases, the intensity is higher in the fjords, e.g., Puyuhuapi, Aysén, and Comau Fjords. The most intense events occur in summer, with

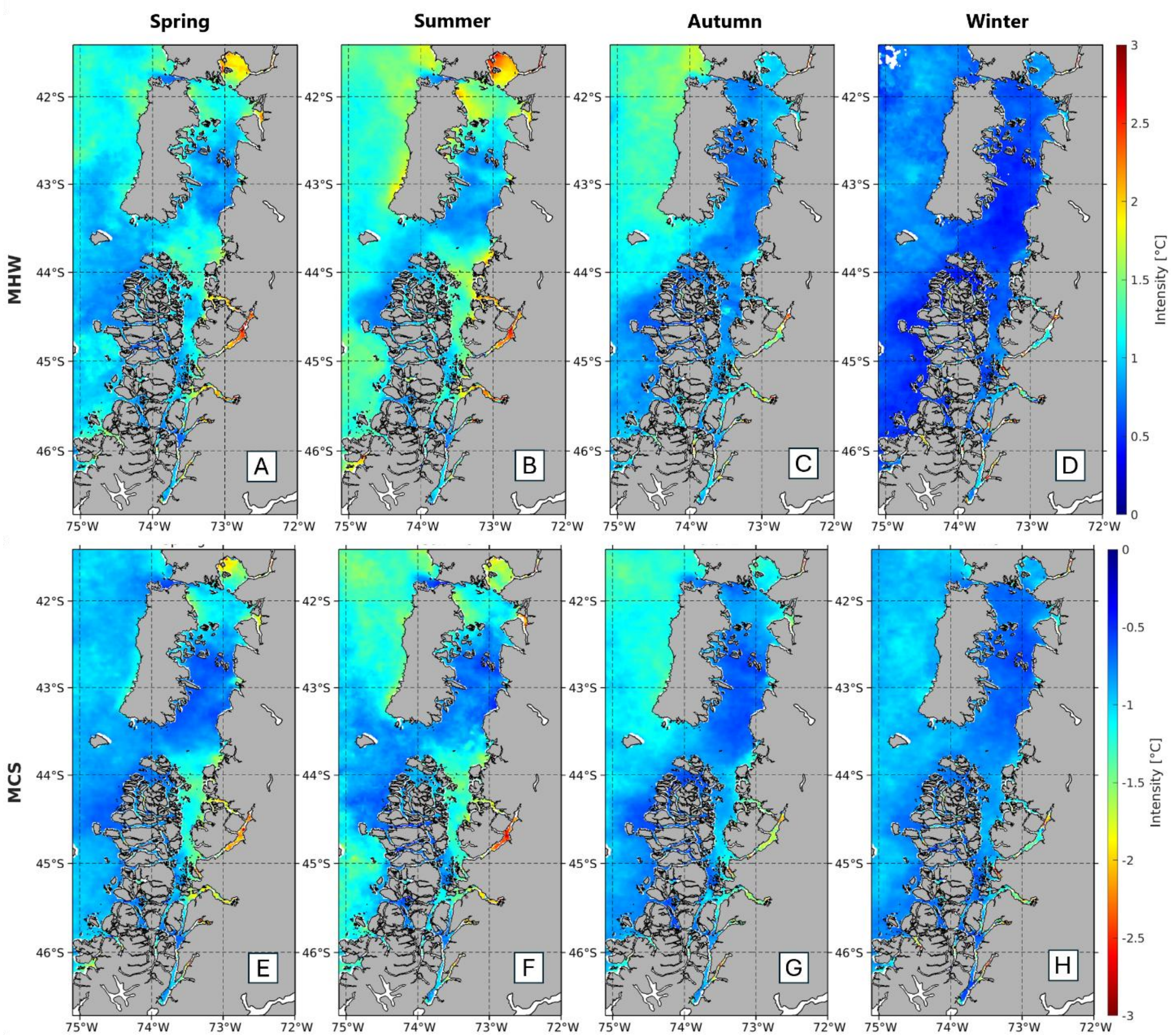

Figure 10: Mean intensity of MHWs (top) and MCSs (bottom) for each season: Spring (A, E), Summer (B, F), Autumn (C, G), Winter (D, H). Representation for the period 2003-2023.

the highest being in Puyuhuapi Fjord for both MHWs and MCS reaching 2,5°C and -2,5°C respectively (Fig. 10B, 10F). Reloncaví Sound, however, experiences more intense MHWs (up to 2.5°C) than MCSs (nearly -2°C). During spring (Fig. 10A, 8E), the Ancud Gulf and the southern part of the Inner Sea of Chiloé are more impacted for both MHWs and MCSs, the Puyuhuapi Fjord being again the region with the highest and lowest values (respectively 2,5°C and -2°C). In autumn the fjords remain the regions of highest intensity, along with the open ocean west of Chiloé Island (Fig. 10C, 10G). The MCS intensity being more intense in summer is quite opposite to what is found in literature. Indeed, MCSs tend to occur more frequently in winter, and are generally less destructive when happening in summer (Schlegel et al., 2021).

3.7 MHWs and MCSs trends

The trend of MHW and MCS metrics were calculated over the period 2003-2023.

The trend of MHW frequency is heterogeneous and mostly basin-linked (Fig. 11A). In the northernmost part of the Inner Sea of Chiloé, Reloncaví Sound and Ancud Gulf, the frequency is yearly increasing by 0.1 events per year, a trend also observed in Moraleda Channel, which is coherent with what was found by Pujol et al. (2022). Puyuhuapi and Aysén Fjords are more significantly impacted, showing a positive trend of between 0.1 and 0.2 events per year. Outside the Inner Sea of Chiloé, a similar trend is observed with an increase in frequency of approximately 0.1 events per year. However, in Corcovado Gulf and along the west coast of Chiloé, the trend is negative, indicating a decrease in MHW frequency over the years, also observed in Pujol et al. (2022). Looking at the MCSs, the trend is more consistent in the Inner Sea of Chiloé: it is negative everywhere with a decrease of between 0.1 and 0.2 events per year (Fig. 11E). A similar pattern is observed west of Chonos Archipelago. West of Chiloé Island, the MCSs tend to increase by about 0.1 events per year.

The trends in MHW mean and maximal intensity display similar patterns (Fig. 11B, 11C). Indeed, the intensity tends to increase in the open ocean west of Chiloé, but not West of Chonos Archipelago and in the southern part of the Inner Sea, from Moraleda Channel to further South, where a decrease is observed. An increasing trend is also evident in Reloncaví Sound, particularly near the mouth and north of Reloncaví Fjord, as well as in the Comau Fjord. Other parts of the study area, i.e. the Ancud and Corcovado Gulfs, Chonos Archipelago and its adjacent waters show a decreasing trend, with the declines observed in the northern Chonos Archipelago and the western Ancud Gulf, at about -0.03°C per year. A distinct demarcation is evident at Guafo Mouth, where a clear separation in trends at its centre. For MCSs, the trends are more pronounced: intensity is increasing everywhere across the study area (Fig. 11F, 11G). This increase seems to be higher inside the Sea of Chiloé, especially in some fjords such as Comau, Aysén and Jacaff Channel, as well at their mouths with maximum intensity rising by 0.06°C per year. Globally, fjords are experiencing warming sea temperature (Pavlov et al., 2013; Aksnes et al., 2019; Skogseth et al., 2020; Bloshkina et al., 2021) as well as Northern Patagonia especially during the last decade (Pujol et al., 2022). Those elements are coherent with an increase in the intensity of MHWs in our study area.

The duration trend of MHWs (Fig. 11D) is overall neutral or slightly decreasing within the Northern Patagonian Fjords, except south of Desertores Islands where a positive trend of more than one day per year, as well as in the southernmost areas of the sea, such as Elefantes Channel and several channels in the Chonos Archipelago. In the open ocean, no clear pattern is apparent,

https://doi.org/10.5194/egusphere-2025-1421
Preprint. Discussion started: 3 April 2025

although much of the western coast of Chiloé shows an increasing trend, occasionally reaching up to 1 day per year. For MCSs

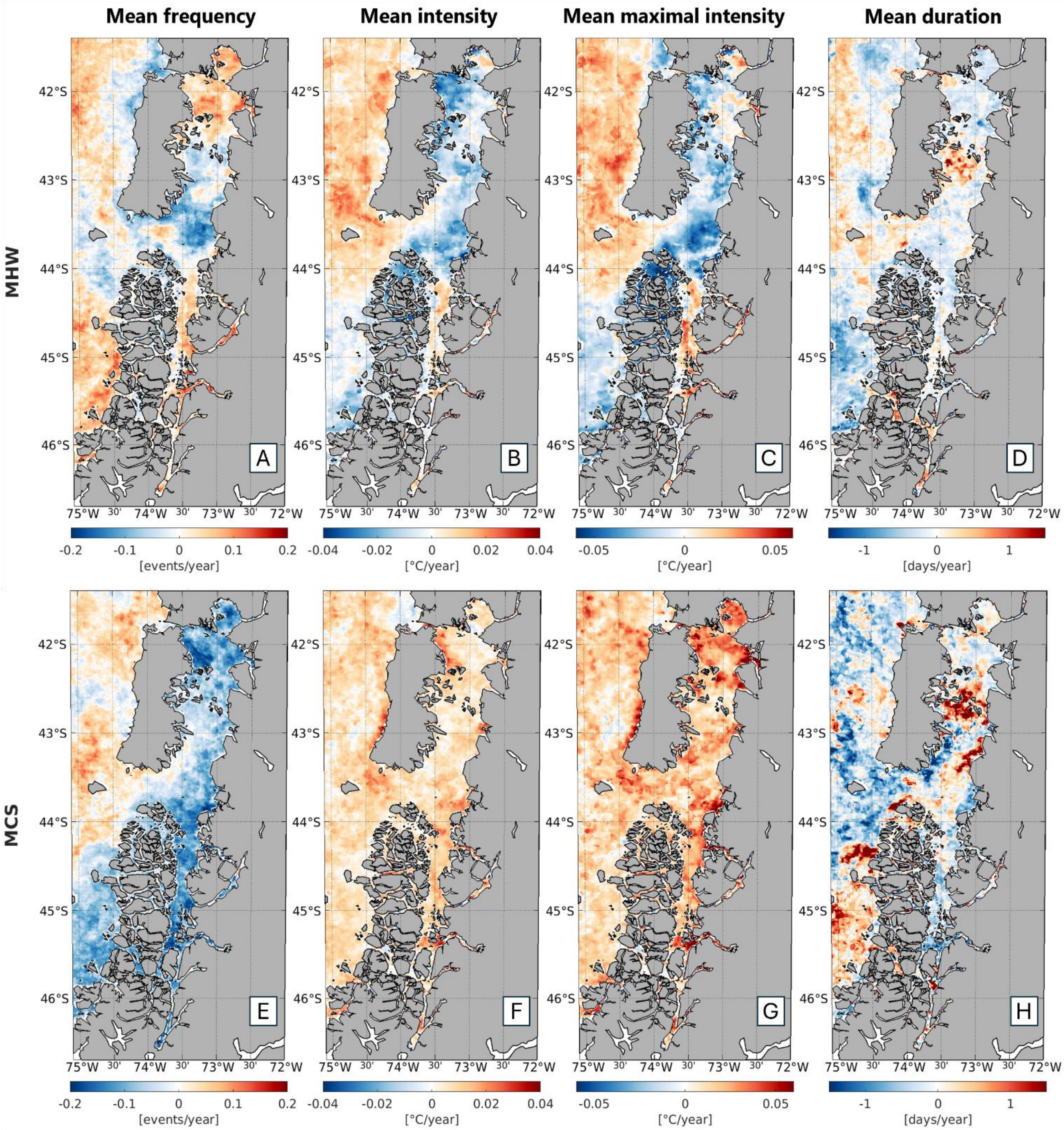

Figure 11: Annual trend for MHWs (top) and MCS (bottom) for different metrics: Frequency (A, E), Mean Intensity (B, F), Mean Maximal Intensity (C, G), Duration (D, H). The trend is expressed in unit per year, which means that for instance in the Reloncaví Sound, the mean intensity of the MCS is increasing by 0.01°C per year. Period: 2003-2023.

https://doi.org/10.5194/egusphere-2025-1421
Preprint. Discussion started: 3 April 2025

(Fig. 11H), a similar patch of increased duration is evident around Desertores Islands, with a rise of 1.5 days per year. West of Chonos Archipelago, an increase of 1 day per year can also be observed. Elsewhere, the trend is more likely in favour of a decrease in the duration by about 1 day per year.

3.8 Examples of remarkable events

3.8.1 Succession of MCSs and MHWs: 2007-2008

Among the different events observed during the last 20 years, some were remarkable by their length, intensity or by the succession of MCSs and MHWs. It is for example the case for the years 2007-2008.

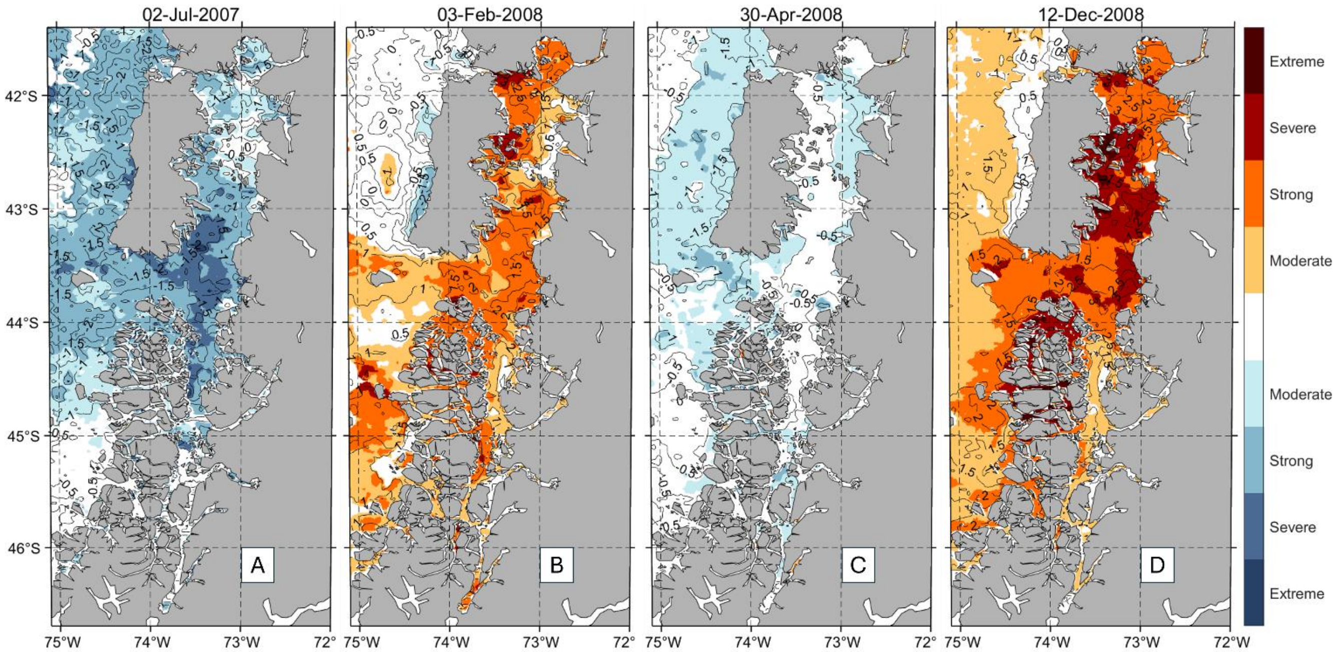

Figure 12: MHWs and MCS categories (respectively shades of reds and blues) on the peak day and the corresponding SST anomalies indicated by the thin black lines.

Between 2007 and 2008, the region experienced successive MCSs and MHWs with brief intervals between events. In May 2007, following an amospheric cold spell, a MCS began around Guafo Mouth, Chonos Archipelago and Moraleda Channel, with temperature anomalies between -0.5°C and -1°C. The MCS continued to spread and by the month of July, most of the study area was affected (Fig. 12A) due to a low-pressure system causing very strong eastward winds and substantial heat loss in the ocean surface, with SST anomalies of -1.5°C. The MCS persisted throughout the austral winter and most of spring, fading in late December. At that time, positive anomalies dominated the study area, though negative anomalies (-1.5°C) persisted along Chiloé Island until January 2008, influenced by a La Niña event which cooled the region and intensified upwelling systems (Muñoz et al., 2023).

On the 22nd of January 2008, a very strong MHW started in Northern Patagonia, driven by increased solar radiation (due to low cloud cover) leading to positive heat flux anomaly. SST anomalies peaked on the 3rd of February with positive anomalies everywhere except along the West coast of Chiloé Island, with +3.5°C in Reloncaví Sound, +3°C west of Ancud Gulf, and exceeded +1.5°C from Reloncaví Sound to the Moraleda Channel (Fig. 12B). This MHW was a category II event in most of the Inner Sea of Chiloé and Southern part of the study area, and reached in localised areas category III (Fig. 12B). The event coincided with an atmospheric heatwave (+3°C on average over the sea) and increased solar radiation (low cloud cover), contributing to a positive heat flux anomaly. It dissipated very quickly in the Inner Sea, due to a low-pressure system in mid-February, bringing some clouds and strong southward winds, dispersing the atmospheric heatwave.

In April, strong eastward winds triggered negative anomalies as low as -1.5°C west of Chiloé Island, inducing a MCS across most of the study area (Fig. 12C). Although this MCS remained relatively weak and largely confined to the Inner Sea, it was persisted during the entire winter.

After a period of weaker winds and positive total net heat flux anomalies, a weak MHW emerged in September 2008 in the open ocean and Guafo Mouth, intermittently persisting and intensifying in December, encomparsing almost the entire study area on the 12th (Fig. 12D). SST anomalies exceeded +1°C across the entire domain, and reached +4°C in the Reloncaví Sound, +3°C on the west side of Ancud Gulf and in the coastal part of the south of Corcovado Gulf. It was classified as category II event in the half North of the Inner Sea and category III around Desertores Islands, Corcovado Gulf and Chonos Archipelago (Fig. 12D). This MHW was linked to a high solar radiation and atmospheric heatwave, resulting in most of the time a positive total heat flux for the ocean. On the 12th of December, the air temperature anomaly above the ocean was +4°C across the entire study area. The MHW dissipated by mid-January as cloud cover increased, reducing solar radiation and air temperature, resulting in negative total heat flux anomalies.

Overall, these events were closely linked to atmospheric conditions, including La Niña, low-pressure systems and atmospheric heatwaves, driving significant SST anomalies in the region.

3.8.2 Strong MHW: 2013

Another notable event was a very strong MHW that occurred during summer 2013. It began by mid-January in the Inner Sea of Chiloé and quickly spread to the open sea, reaching its peak between the 7th and 10th of February, with temperature anomalies of 4°C in Reloncaví Sound, Puyuhuapi and Aysén Fjords, 3°C in the north of the Gulf of Ancud, Comau Fjord and Moraleda Channel, and superior to 1°C in the remaining parts of the Northern Patagonia (Fig. 13A). It was classified as a category II in most areas, with localised category III (Fig. 13A). Notably, the west shore of Chiloé Island remained unaffected likely due to upwellings (Narváez et al., 2019; Pérez-Santos et al., 2019). The event then vanished in about 10 days but persisted west of Chonos Archipelago until May.

This MHW coincided with a very intense atmospheric heatwave that started a few days before the MHW, with temperature anomalies exceeding +10°C over the continent, +5°C over parts of the Inner Sea and +3°C over the open ocean. Both marine and atmospheric heatwaves were accompanied by an unusually low cloud cover, increasing solar radiation. Wind speed showed no distinct pattern contributed to the MHW; in fact, winds were stronger than usual and directed northward when the event began (Fig. not shown).

3.8.3 Long lasting period of MHWs: 2016-2017

The years 2016-2017 experienced prolonged MHW conditions, with events spanning from late December 2015 to early Arpil 2016 and mid-May 2016 to late July 2017, interrupted by just one month without MHW activity during austral summer. The first MHW began west of Chiloé Island in late 2015, quickly spreading to the Inner Sea by January 2016, driven by strong positive solar radiation anomalies (>+180W/m² on the 7th of January 2016), exceptionally low cloud cover, and positive air temperature anomalies. By the 20th of January, the entire area was experiencing MHW with SST anomalies of +1.5°C to +2°C, peaking at +3°C in Puyuhuapi and Aysén Fjords (Fig. 13B). Strong winds in February induced negative heat flux, weakening the MHW which fully dissipated by late February, except south of Desertores Islands where it lasted until early April.

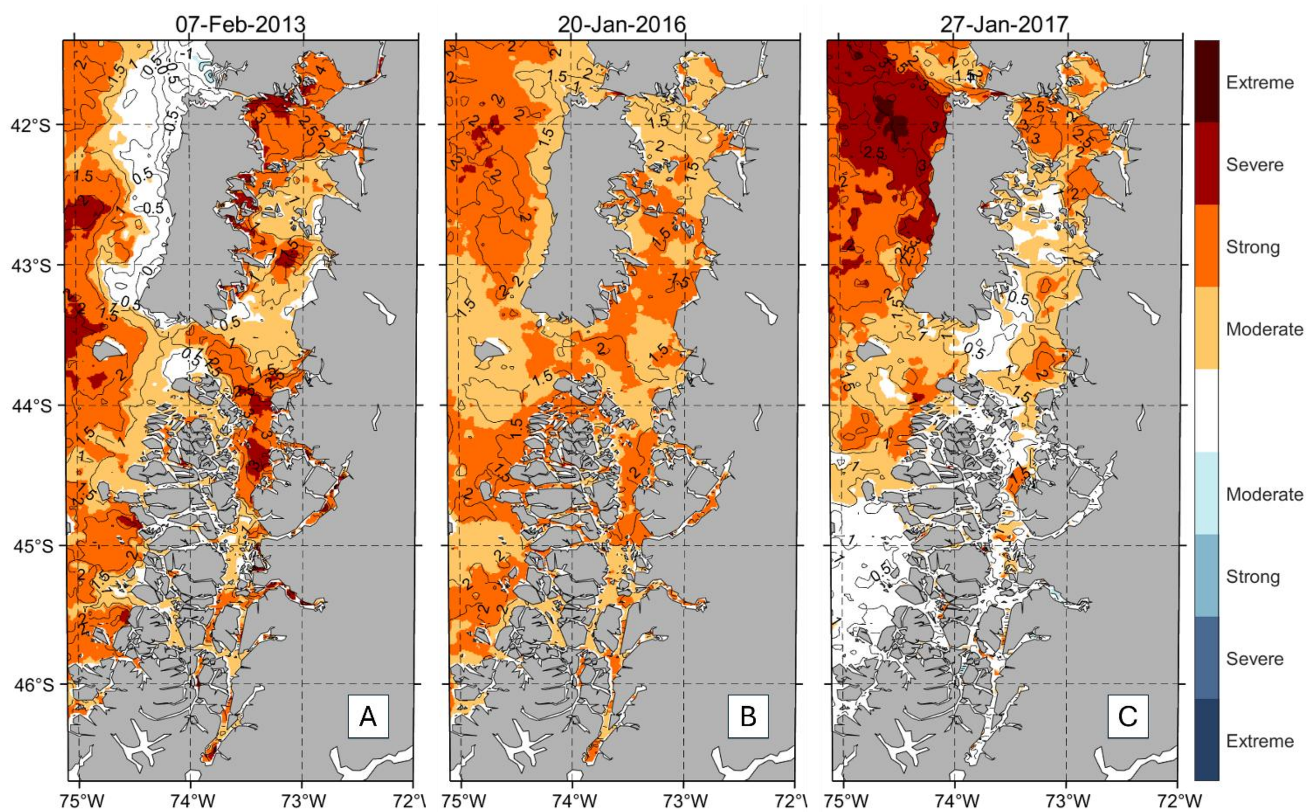

Figure 13: MHWs and MCS categories (respectively shades of reds and blues) on the peak day and the corresponding SST anomalies indicated by the thin black lines.

March and April were hit by various events of strong winds and strongly negative total net heat flux anomalies. However, by mid-May, weakened winds led to positive heat flux, triggering another MHW near Desertores Islands, gradually spreading north, west and south by June. Anticyclonic conditions accompanied the MHW, but declined in July with the arrival of a low-pressure system. Summer and spring 2016 were marked by toxic algal blooms attributed to the atmospheric heatwave and

https://doi.org/10.5194/egusphere-2025-1421
Preprint. Discussion started: 3 April 2025

reduced rainfall (Garreaud, 2018a; León-Muñoz et al., 2018; Díaz and Figueroa, 2023) and causing strong economic losses in aquaculture farms (León-Muñoz et al., 2018), coinciding with the MHWs observed here.

Throughout winter and spring 2016, the MHW persisted intermittently along the continental east coast of the Inner Sea, with SST anomalies around +0.5°C. It pulsed sporadically across the Inner Sea until almost vanishing in December. However, a new intense MHW emerged west of Chiloé Island at the end of December, classified as category IV. The MHW spread to the northern half of the study area, and peaked on the 27th of January 2017 with SST anomalies of +3°C at its centre (Fig. 13C). Similar anomalies appeared in Ancud Gulf and Reloncaví Sound but were classified only as category II events due to the greater temperature variability in these areas in summer.

The intense 2017 event was linked to positive heat flux and atmospheric heatwave, though these conditions alone could not fully explain its strength compared to previous events in 2008 and 2013. The 2016-2017 MHWs align with those described by Pujol et al. (2022), noting winter 2016 and particularly intense ones west of Northern Patagonia in summer 2017.

The MHW shrank but pulsed again in the southern Inner Sea in late February, continuing intermittently in March, April and May around the Chonos Archipelago and Desertores Islands before fully dissipating by the end of July.

The years 2016 and 2017 were impacted by a particularly strong El Niño event, linked to reduced precipitations, atmospheric heatwaves and harmful algal blooms (Garreaud, 2018a, b), but also registered as being part of MHW triggering around Chilean Patagonia (Pujol et al., 2022).

4 Conclusion

In this study, we presented a new methodology for detecting MHWs and MCSs. It involves basing the climatology on long-term in situ data (1948-2022) while calculating the threshold and the daily temperature using satellite data over the study period of 2003 to 2023.

A key issue in MHW and MCS detection is that the climatology should be based on long-term data to take into account multi-decadal temperature trends. Although the climatology is generally calculated using satellite data, this was not feasible for our study area, the Chilean Northern Patagonia. Indeed, long-term satellite data lack the spatial resolution required to resolve intricate fjords, gulfs and channels of Northern Patagonia. Consequently, we decided to use in situ data to build the climatology, incorporating over 3 million sparse samples. These data were interpolated spatially and temporally to produce a monthly and daily climatology of the sea temperature of the Northern Patagonia with a spatial resolution of 900m at 32 different depths. This climatology was then used to detect MHWs and MCSs at very high resolution, appearing consistent with the available literature.

This methodology enabled us to detect surface MHWs and MCSs individually and to analyse their different metrics. We found that every location experiences MHW and MCS at least once a year, and that they do not show similar or opposite spatial patterns. MCSs are particularly frequent in the northern part of Northern Patagonia, more precisely in Ancud and Reloncaví Gulfs, as well as Comau fjord, whereas MHWs are more frequent in the southern part of Northern Patagonia. Regarding the mean intensity, both MHWs and MCSs are significantly more intense in the most enclosed basins, such as Reloncaví Sound, Comau and Puyuhuapi Fjords. MCS duration is also generally longer (between 10 and 25 days) than MHWs (10 to 20 days). Seasonal patterns reveal that MHWs are more frequent in summer and absent in winter, while MCSs are more frequent in winter and absent in summer. When looking at the intensity, both phenomena exhibit similar seasonal patterns, tending to be more intense during summer months.

By analysing several case studies, we observed that in Northern Patagonia, MHWs can be triggered and/or accompanied by atmospheric heatwaves, reduced winds, reduced cloud cover and positive El Niño Southern Oscillation phase. Conversely, MCSs are triggered by low-pressure systems, stronger winds and negative phase of El Niño Southern Oscillation (La Niña).

Trends over the 2003-2023 period indicate that MCSs are becoming less frequent but more intense, whereas MHWs are becoming more frequent (except in Corcovado Gulf) but less intense. The intensity trend of MCSs is positive everywhere and particularly homogeneous, in contrast to the MHW trend which shows more basin-specific variability, both positive and negative. Regarding duration, MCSs are becoming longer around Desertores Islands and Chonos Archipelago, whereas MHWs are very slightly becoming shorter overall except around Desertores Islands where they also tend to be longer.

This study highlights the importance of examining MHWs and MCSs at high resolution in coastal environment: these events are far from homogeneous across the Northern Patagonia, as is likely the case for other complex coastal regions. Enclosed basins such as Reloncaví Sound, Puyuhuapi and Comau Fjords, are more likely to be prone to intense events, whereas Corcovado Gulf appears relatively resilient, with low intensity events. High-resolution detection of these events is crucial for gaining a comprehensive understanding of MHWs and MCSs dynamics in coastal areas, enabling better analysis of their consequences on ecosystems and assisting local stakeholders in mitigating such events.

5 Appendix

Table A 1: Quantity of samples used for the climatology validation. Distinction between mooring in situ data and "not mooring" in situ data is done because although mooring provides large amounts of data, they represent a fix point, contrary to other methods of sampling that give spatially sparse results.

Month	All in situ data between 0m and 1m depth	Mooring data	Quantity of data kept apart for validation (5%)	All in situ data that are not from moorings	Quantity of data kept apart for validation (5%)
Jan	8792	8693	435	99	5
Feb	14680	13685	684	995	50
Mar	13921	13711	686	210	11
Apr	8534	8373	419	161	8
May	10081	9478	474	603	30
Jun	9409	9077	454	332	17
Jul	9825	9331	467	494	25
Aug	9022	8557	428	465	23
Sep	10289	9540	477	749	37
Oct	9659	9174	459	485	24
Nov	8712	7701	385	1011	51
Dec	9238	9020	451	218	11

Author contribution

C.P. Main researcher, main writer.

A.B. Co-supervisor of research, contribution for the research and contribution to the manuscript's redaction.

I.P-S. Provided in situ data, contribution to the research, contributed to the manuscript's redaction.

P.M-L. Provided in situ data and contributed to the manuscript's redaction.

A.A-A. Co- supervisor, contribution to the research, and contributed to the manuscript's redaction.

Data availability

The monthly and daily climatologies described in Sections 2.2 and 3.2 are available on Zenodo (DOI: https://doi.org/10.5281/zenodo.14845077) and can be freely used for any purpose. The threshold dataset described in Sections 2.3 and 3.3 and the SST dataset described in Sections 2.3 and 3.4 are also available on the same page; however we recommend to use it only for the detection of MHWs and MCSs, in addition to the daily climatology.

Figures fully describing the monthly climatology at every depth are available in the supplementary material.

https://doi.org/10.5194/egusphere-2025-1421
Preprint. Discussion started: 3 April 2025

The list, description and sources/DOIs of all the in situ data used for the construction of the climatology (Section 2.2) are also available in the supplementary material.

Competing interests

The authors declare that they have no conflicts of interest, except Aida Alvera-Azcárate, editor of the special issue on Ocean Extremes (55th International Liège Colloquium).

Financial supports

C. Pujol received financial support from the FRS-FNRS (Fonds de la Recherche Scientifique de Belgique, Communauté Française de Belgique) through funding the position of AB and with a doctoral FRIA grant for CP.

References

Aguirre, C., Pizarro, Ó., Strub, P. T., Garreaud, R., and Barth, J. A.: Seasonal dynamics of the near-surface alongshore flow off central Chile, J. Geophys. Res., 117, 2011JC007379, https://doi.org/10.1029/2011JC007379, 2012.

Aguirre, C., Rojas, M., Garreaud, R. D., and Rahn, D. A.: Role of synoptic activity on projected changes in upwelling-favourable winds at the ocean's eastern boundaries, npj Clim Atmos Sci, 2, 44, https://doi.org/10.1038/s41612-019-0101-9, 2019.

Aksnes, D. L., Aure, J., Johansen, P.-O., Johnsen, G. H., and Vea Salvanes, A. G.: Multi-decadal warming of Atlantic water and associated decline of dissolved oxygen in a deep fjord, Estuarine, Coastal and Shelf Science, 228, 106392, https://doi.org/10.1016/j.ecss.2019.106392, 2019.

Alvera-Azcárate, A., Barth, A., Rixen, M., and Beckers, J. M.: Reconstruction of incomplete oceanographic data sets using empirical orthogonal functions: application to the Adriatic Sea surface temperature, Ocean Modelling, 9, 325–346, https://doi.org/10.1016/j.ocemod.2004.08.001, 2005.

Alvera-Azcárate, A., Barth, A., Sirjacobs, D., Lenartz, F., and Beckers, J. M.: Data Interpolating Empirical Orthogonal Functions (DINEOF): a tool for geophysical data analyses, Medit. Mar. Sci., 12, 5, https://doi.org/10.12681/mms.64, 2011.

Ancapichún, S. and Garcés-Vargas, J.: Variability of the Southeast Pacific Subtropical Anticyclone and its impact on sea surface temperature off north-central Chile, Cienc. Mar., 41, 1–20, https://doi.org/10.7773/cm.v41i1.2338, 2015.

Arafeh-Dalmau, N., Montaño-Moctezuma, G., Martínez, J. A., Beas-Luna, R., Schoeman, D. S., and Torres-Moye, G.: Extreme Marine Heatwaves Alter Kelp Forest Community Near Its Equatorward Distribution Limit, Front. Mar. Sci., 6, 499, https://doi.org/10.3389/fmars.2019.00499, 2019.

Barbeaux, S. J., Holsman, K., and Zador, S.: Marine Heatwave Stress Test of Ecosystem-Based Fisheries Management in the Gulf of Alaska Pacific Cod Fishery, Front. Mar. Sci., 7, 703, https://doi.org/10.3389/fmars.2020.00703, 2020.

Barth, A., Beckers, J.-M., Troupin, C., Alvera-Azcárate, A., and Vandenbulcke, L.: divand-1.0: n-dimensional variational data analysis for ocean observations, Geosci. Model Dev., 7, 225–241, https://doi.org/10.5194/gmd-7-225-2014, 2014.

Bayoumy, M., Nilsen, F., and Skogseth, R.: Marine Heatwaves Characteristics in the Barents Sea Based on High Resolution Satellite Data (1982–2020), Front. Mar. Sci., 9, 821646, https://doi.org/10.3389/fmars.2022.821646, 2022.

Bloshkina, E. V., Pavlov, A. K., and Filchuk, K.: Warming of Atlantic Water in three west Spitsbergen fjords: recent patterns and century-long trends, Polar Research, 40, https://doi.org/10.33265/polar.v40.5392, 2021.

Brauko, K. M., Cabral, A., Costa, N. V., Hayden, J., Dias, C. E. P., Leite, E. S., Westphal, R. D., Mueller, C. M., Hall-Spencer, J. M., Rodrigues, R. R., Rörig, L. R., Pagliosa, P. R., Fonseca, A. L., Alarcon, O. E., and Horta, P. A.: Marine Heatwaves, Sewage and Eutrophication Combine to Trigger Deoxygenation and Biodiversity Loss: A SW Atlantic Case Study, Front. Mar. Sci., 7, 590258, https://doi.org/10.3389/fmars.2020.590258, 2020.

Buchan, S. J., Pérez-Santos, I., Narváez, D., Castro, L., Stafford, K. M., Baumgartner, M. F., Valle-Levinson, A., Montero, P., Gutiérrez, L., Rojas, C., Daneri, G., and Neira, S.: Intraseasonal variation in southeast Pacific blue whale acoustic presence, zooplankton backscatter, and oceanographic variables on a feeding ground in Northern Chilean Patagonia, Progress in Oceanography, 199, 102709, https://doi.org/10.1016/j.pocean.2021.102709, 2021.

Burger, F. A., Terhaar, J., and Frölicher, T. L.: Compound marine heatwaves and ocean acidity extremes, Nat Commun, 13, 4722, https://doi.org/10.1038/s41467-022-32120-7, 2022.

Calvete, C. and Sobarzo, M.: Quantification of the surface brackish water layer and frontal zones in southern Chilean fjords between Boca del Guafo (43°30′S) and Estero Elefantes (46°30′S), Continental Shelf Research, 31, 162–171, https://doi.org/10.1016/j.csr.2010.09.013, 2011.

Capotondi, A., Rodrigues, R. R., Sen Gupta, A., Benthuysen, J. A., Deser, C., Frölicher, T. L., Lovenduski, N. S., Amaya, D. J., Le Grix, N., Xu, T., Hermes, J., Holbrook, N. J., Martinez-Villalobos, C., Masina, S., Roxy, M. K., Schaeffer, A., Schlegel, R. W., Smith, K. E., and Wang, C.: A global overview of marine heatwaves in a changing climate, Commun Earth Environ, 5, 701, https://doi.org/10.1038/s43247-024-01806-9, 2024.

Castillo, M. I., Cifuentes, U., Pizarro, O., Djurfeldt, L., and Caceres, M.: Seasonal hydrography and surface outflow in a fjord with a deep sill: the Reloncaví fjord, Chile, Ocean Sci., 12, 533–544, https://doi.org/10.5194/os-12-533-2016, 2016.

Cheng, Y., Zhang, M., Song, Z., Wang, G., Zhao, C., Shu, Q., Zhang, Y., and Qiao, F.: A quantitative analysis of marine heatwaves in response to rising sea surface temperature, Science of The Total Environment, 881, 163396, https://doi.org/10.1016/j.scitotenv.2023.163396, 2023.

Cheung, W. W. L. and Frölicher, T. L.: Marine heatwaves exacerbate climate change impacts for fisheries in the northeast Pacific, Sci Rep, 10, 6678, https://doi.org/10.1038/s41598-020-63650-z, 2020.

Cook, F., Smith, R. O., Roughan, M., Cullen, N. J., Shears, N., and Bowen, M.: Marine heatwaves in shallow coastal ecosystems are coupled with the atmosphere: Insights from half a century of daily in situ temperature records, Front. Clim., 4, 1012022, https://doi.org/10.3389/fclim.2022.1012022, 2022.

Dabulevičienė, T. and Servaitė, I.: Characteristics of Marine Heatwaves in the Southeastern Baltic Sea Based on Long-Term In Situ and Satellite Observations, JMSE, 12, 1109, https://doi.org/10.3390/jmse12071109, 2024.

Dalton, S. J., Carroll, A. G., Sampayo, E., Roff, G., Harrison, P. L., Entwistle, K., Huang, Z., Salih, A., and Diamond, S. L.: Successive marine heatwaves cause disproportionate coral bleaching during a fast phase transition from El Niño to La Niña, Science of The Total Environment, 715, 136951, https://doi.org/10.1016/j.scitotenv.2020.136951, 2020.

Díaz, P. A. and Figueroa, R. I.: Toxic Algal Bloom Recurrence in the Era of Global Change: Lessons from the Chilean Patagonian Fjords, Microorganisms, 11, 1874, https://doi.org/10.3390/microorganisms11081874, 2023.

Díaz, P. A., Pérez-Santos, I., Basti, L., Garreaud, R., Pinilla, E., Barrera, F., Tello, A., Schwerter, C., Arenas-Uribe, S., Soto-Riquelme, C., Navarro, P., Díaz, M., Álvarez, G., Linford, P. M., Altamirano, R., Mancilla-Gutiérrez, G., Rodríguez-Villegas, C., and Figueroa, R. I.: The impact of local and climate change drivers on the formation, dynamics, and potential recurrence of a massive fish-killing microalgal bloom in Patagonian fjord, Science of The Total Environment, 865, 161288, https://doi.org/10.1016/j.scitotenv.2022.161288, 2023.

Filbee-Dexter, K., Wernberg, T., Grace, S. P., Thormar, J., Fredriksen, S., Narvaez, C. N., Feehan, C. J., and Norderhaug, K. M.: Marine heatwaves and the collapse of marginal North Atlantic kelp forests, Sci Rep, 10, 13388, https://doi.org/10.1038/s41598-020-70273-x, 2020.

Frölicher, T. L., Fischer, E. M., and Gruber, N.: Marine heatwaves under global warming, Nature, 560, 360–364, https://doi.org/10.1038/s41586-018-0383-9, 2018.

Garrabou, J., Gómez-Gras, D., Medrano, A., Cerrano, C., Ponti, M., Schlegel, R., Bensoussan, N., Turicchia, E., Sini, M., Gerovasileiou, V., Teixido, N., Mirasole, A., Tamburello, L., Cebrian, E., Rilov, G., Ledoux, J., Souissi, J. B., Khamassi, F., Ghanem, R., Benabdi, M., Grimes, S., Ocaña, O., Bazairi, H., Hereu, B., Linares, C., Kersting, D. K., La Rovira, G., Ortega, J., Casals, D., Pagès-Escolà, M., Margarit, N., Capdevila, P., Verdura, J., Ramos, A., Izquierdo, A., Barbera, C., Rubio-Portillo, E., Anton, I., López-Sendino, P., Díaz, D., Vázquez-Luis, M., Duarte, C., Marbà, N., Aspillaga, E., Espinosa, F., Grech, D., Guala, I., Azzurro, E., Farina, S., Cristina Gambi, M., Chimienti, G., Montefalcone, M., Azzola, A., Mantas, T. P., Fraschetti, S., Ceccherelli, G., Kipson, S., Bakran-Petricioli, T., Petricioli, D., Jimenez, C., Katsanevakis, S., Kizilkaya, I. T., Kizilkaya, Z., Sartoretto, S., Elodie, R., Ruitton, S., Comeau, S., Gattuso, J., and Harmelin, J.: Marine heatwaves drive recurrent mass mortalities in the Mediterranean Sea, Global Change Biology, 28, 5708–5725, https://doi.org/10.1111/gcb.16301, 2022.

Garreaud, R.: Record-breaking climate anomalies lead to severe drought and environmental disruption in western Patagonia in 2016, Clim. Res., 74, 217–229, https://doi.org/10.3354/cr01505, 2018a.

Garreaud, R. D.: A plausible atmospheric trigger for the 2017 coastal El Niño, Intl Journal of Climatology, 38, https://doi.org/10.1002/joc.5426, 2018b.

Garreaud, R. D. and Aceituno, P.: Atmospheric Circulation and Climatic Variability, Thephysical geography of South America, 45, 2007.

Gruber, N., Boyd, P. W., Frölicher, T. L., and Vogt, M.: Biogeochemical extremes and compound events in the ocean, Nature, 600, 395–407, https://doi.org/10.1038/s41586-021-03981-7, 2021.

Guo, X., Gao, Y., Zhang, S., Wu, L., Chang, P., Cai, W., Zscheischler, J., Leung, L. R., Small, J., Danabasoglu, G., Thompson, L., and Gao, H.: Threat by marine heatwaves to adaptive large marine ecosystems in an eddy-resolving model, Nat. Clim. Chang., 12, 179–186, https://doi.org/10.1038/s41558-021-01266-5, 2022.

Hersbach, H., Bell, B., Berrisford, P., Biavati, G., Horányi, A., Muñoz Sabater, J., Nicolas, J., Peubey, C., Radu, R., Rozum, I., Schepers, D., Simmons, A., Soci, C., Dee, D., and Thépaut, J.-N.: ERA5 hourly data on single levels from 1940 to present. (Copernicus Climate Change Service (C3S) Climate Data Store (CDS)), https://doi.org/10.24381/cds.adbb2d47, 2023.

https://doi.org/10.5194/egusphere-2025-1421
Preprint. Discussion started: 3 April 2025

Hobday, A., Alexander, L. V., Perkins, S. E., Smale, D. A., Straub, S. C., Oliver, E. C. J., Benthuysen, J. A., Burrows, M. T., Donat, M. G., Feng, M., Holbrook, N. J., Moore, P. J., Scannell, H. A., Sen Gupta, A., and Wernberg, T.: A hierarchical approach to defining marine heatwaves, Progress in Oceanography, 141, 227–238, https://doi.org/10.1016/j.pocean.2015.12.014, 2016.

Hobday, A., Oliver, E., Sen Gupta, A., Benthuysen, J., Burrows, M., Donat, M., Holbrook, N., Moore, P., Thomsen, M., Wernberg, T., and Smale, D.: Categorizing and Naming Marine Heatwaves, Oceanog, 31, https://doi.org/10.5670/oceanog.2018.205, 2018.

Holbrook, N. J., Scannell, H. A., Sen Gupta, A., Benthuysen, J. A., Feng, M., Oliver, E. C. J., Alexander, L. V., Burrows, M. T., Donat, M. G., Hobday, A. J., Moore, P. J., Perkins-Kirkpatrick, S. E., Smale, D. A., Straub, S. C., and Wernberg, T.: A global assessment of marine heatwaves and their drivers, Nat Commun, 10, 2624, https://doi.org/10.1038/s41467-019-10206-z, 2019.

Holbrook, N. J., Sen Gupta, A., Oliver, E. C. J., Hobday, A. J., Benthuysen, J. A., Scannell, H. A., Smale, D. A., and Wernberg, T.: Keeping pace with marine heatwaves, Nat Rev Earth Environ, 1, 482–493, https://doi.org/10.1038/s43017-020-0068-4, 2020.

Huang, B., Liu, C., Banzon, V., Freeman, E., Graham, G., Hankins, B., Smith, T., and Zhang, H.-M.: Improvements of the Daily Optimum Interpolation Sea Surface Temperature (DOISST) Version 2.1, Journal of Climate, 34, 2923–2939, https://doi.org/10.1175/JCLI-D-20-0166.1, 2021.

Huang, Z., Feng, M., Dalton, S. J., and Carroll, A. G.: Marine heatwaves in the Great Barrier Reef and Coral Sea: their mechanisms and impacts on shallow and mesophotic coral ecosystems, Science of The Total Environment, 908, 168063, https://doi.org/10.1016/j.scitotenv.2023.168063, 2024.

Jackson, J. M., Johnson, G. C., Dosser, H. V., and Ross, T.: Warming From Recent Marine Heatwave Lingers in Deep British Columbia Fjord, Geophysical Research Letters, 45, 9757–9764, https://doi.org/10.1029/2018GL078971, 2018.

Jordà-Molina, È., Renaud, P. E., Silberberger, M. J., Sen, A., Bluhm, B. A., Carroll, M. L., Ambrose, W. G., Cottier, F., and Reiss, H.: Seafloor warm water temperature anomalies impact benthic macrofauna communities of a high-Arctic cold-water fjord, Marine Environmental Research, 189, 106046, https://doi.org/10.1016/j.marenvres.2023.106046, 2023.

Khangaonkar, T., Nugraha, A., Yun, S. K., Premathilake, L., Keister, J. E., and Bos, J.: Propagation of the 2014–2016 Northeast Pacific Marine Heatwave Through the Salish Sea, Front. Mar. Sci., 8, 787604, https://doi.org/10.3389/fmars.2021.787604, 2021.

Kuroda, H., Azumaya, T., Setou, T., and Hasegawa, N.: Unprecedented Outbreak of Harmful Algae in Pacific Coastal Waters off Southeast Hokkaido, Japan, during Late Summer 2021 after Record-Breaking Marine Heatwaves, JMSE, 9, 1335, https://doi.org/10.3390/jmse9121335, 2021.

Laufkötter, C., Zscheischler, J., and Frölicher, T. L.: High-impact marine heatwaves attributable to human-induced global warming, Science, 369, 1621–1625, https://doi.org/10.1126/science.aba0690, 2020.

León-Muñoz, J., Marcé, R., and Iriarte, J.: Influence of hydrological regime of an Andean river on salinity, temperature and oxygen in a Patagonia fjord, Chile, New Zealand Journal of Marine and Freshwater Research, 47, 515–528, https://doi.org/10.1080/00288330.2013.802700, 2013.

León-Muñoz, J., Urbina, M. A., Garreaud, R., and Iriarte, J. L.: Hydroclimatic conditions trigger record harmful algal bloom in western Patagonia (summer 2016), Sci Rep, 8, 1330, https://doi.org/10.1038/s41598-018-19461-4, 2018.

Linford, P., Pérez-Santos, I., Montes, I., Dewitte, B., Buchan, S., Narváez, D., Saldías, G., Pinilla, E., Garreaud, R., Díaz, P., Schwerter, C., Montero, P., Rodríguez-Villegas, C., Cáceres-Soto, M., Mancilla-Gutiérrez, G., and Altamirano, R.: Recent Deoxygenation of Patagonian Fjord Subsurface Waters Connected to the Peru–Chile Undercurrent and Equatorial Subsurface Water Variability, Global Biogeochemical Cycles, 37, e2022GB007688, https://doi.org/10.1029/2022GB007688, 2023.

Linford, P., Pérez-Santos, I., Montero, P., Díaz, P. A., Aracena, C., Pinilla, E., Barrera, F., Castillo, M., Alvera-Azcárate, A., Alvarado, M., Soto, G., Pujol, C., Schwerter, C., Arenas-Uribe, S., Navarro, P., Mancilla-Gutiérrez, G., Altamirano, R., San Martín, J., and Soto-Riquelme, C.: Oceanographic processes driving low-oxygen conditions inside Patagonian fjords, Biogeosciences, 21, 1433–1459, https://doi.org/10.5194/bg-21-1433-2024, 2024.

Magel, C. L., Chan, F., Hessing-Lewis, M., and Hacker, S. D.: Differential Responses of Eelgrass and Macroalgae in Pacific Northwest Estuaries Following an Unprecedented NE Pacific Ocean Marine Heatwave, Front. Mar. Sci., 9, 838967, https://doi.org/10.3389/fmars.2022.838967, 2022.

Marin, M., Bindoff, N. L., Feng, M., and Phillips, H. E.: Slower Long-Term Coastal Warming Drives Dampened Trends in Coastal Marine Heatwave Exposure, JGR Oceans, 126, e2021JC017930, https://doi.org/10.1029/2021JC017930, 2021.

Maturana-Martínez, C., Fernández, C., González, H. E., and Galand, P. E.: Different Active Microbial Communities in Two Contrasted Subantarctic Fjords, Front. Microbiol., 12, 620220, https://doi.org/10.3389/fmicb.2021.620220, 2021.

Maulu, S., Hasimuna, O. J., Haambiya, L. H., Monde, C., Musuka, C. G., Makorwa, T. H., Munganga, B. P., Phiri, K. J., and Nsekanabo, J. D.: Climate Change Effects on Aquaculture Production: Sustainability Implications, Mitigation, and Adaptations, Front. Sustain. Food Syst., 5, 609097, https://doi.org/10.3389/fsufs.2021.609097, 2021.

Mazzini, P. L. F. and Pianca, C.: Marine Heatwaves in the Chesapeake Bay, Front. Mar. Sci., 8, 750265, https://doi.org/10.3389/fmars.2021.750265, 2022.

McCabe, R. M., Hickey, B. M., Kudela, R. M., Lefebvre, K. A., Adams, N. G., Bill, B. D., Gulland, F. M. D., Thomson, R. E., Cochlan, W. P., and Trainer, V. L.: An unprecedented coastwide toxic algal bloom linked to anomalous ocean conditions, Geophysical Research Letters, 43, https://doi.org/10.1002/2016GL070023, 2016.

Merkouriadi, I. and Leppäranta, M.: Influence of sea ice on the seasonal variability of hydrography and heat content in Tvärminne, Gulf of Finland, Ann. Glaciol., 56, 274–284, https://doi.org/10.3189/2015AoG69A003, 2015.

Mignot, A., Von Schuckmann, K., Landschützer, P., Gasparin, F., Van Gennip, S., Perruche, C., Lamouroux, J., and Amm, T.: Decrease in air-sea CO2 fluxes caused by persistent marine heatwaves, Nat Commun, 13, 4300, https://doi.org/10.1038/s41467-022-31983-0, 2022.

Muñoz, R., Vergara, O. A., Figueroa, P. A., Mardones, P., Sobarzo, M., and Saldías, G. S.: On the phenology of coastal upwelling off central-southern Chile, Dynamics of Atmospheres and Oceans, 104, 101405, https://doi.org/10.1016/j.dynatmoce.2023.101405, 2023.

Narváez, D. A., Vargas, C. A., Cuevas, L. A., García-Loyola, S. A., Lara, C., Segura, C., Tapia, F. J., and Broitman, B. R.: Dominant scales of subtidal variability in coastal hydrography of the Northern Chilean Patagonia, Journal of Marine Systems, 193, 59–73, https://doi.org/10.1016/j.jmarsys.2018.12.008, 2019.

NASA OBPG: MODIS Aqua Global Level 3 Mapped SST. Ver. 2019.0., https://doi.org/10.5067/MODAM-8D4N9, 2020.

Oliver, E. C. J., Donat, M. G., Burrows, M. T., Moore, P. J., Smale, D. A., Alexander, L. V., Benthuysen, J. A., Feng, M., Sen Gupta, A., Hobday, A. J., Holbrook, N. J., Perkins-Kirkpatrick, S. E., Scannell, H. A., Straub, S. C., and Wernberg, T.: Longer

https://doi.org/10.5194/egusphere-2025-1421
Preprint. Discussion started: 3 April 2025

and more frequent marine heatwaves over the past century, Nat Commun, 9, 1324, https://doi.org/10.1038/s41467-018-03732-9, 2018.

Pavlov, A. K., Tverberg, V., Ivanov, B. V., Nilsen, F., Falk-Petersen, S., and Granskog, M. A.: Warming of Atlantic Water in two west Spitsbergen fjords over the last century (1912–2009), Polar Research, 32, 11206, https://doi.org/10.3402/polar.v32i0.11206, 2013.

Pérez-Santos, I., Garcés-Vargas, J., Schneider, W., Ross, L., Parra, S., and Valle-Levinson, A.: Double-diffusive layering and mixing in Patagonian fjords, Progress in Oceanography, 129, 35–49, https://doi.org/10.1016/j.pocean.2014.03.012, 2014.

Pérez-Santos, I., Seguel, R., Schneider, W., Linford, P., Donoso, D., Navarro, E., Amaya-Cárcamo, C., Pinilla, E., and Daneri, G.: Synoptic-scale variability of surface winds and ocean response to atmospheric forcing in the eastern austral Pacific Ocean, Ocean Sci., 15, 1247–1266, https://doi.org/10.5194/os-15-1247-2019, 2019.

Pérez-Santos, I., Díaz, P. A., Silva, N., Garreaud, R., Montero, P., Henríquez-Castillo, C., Barrera, F., Linford, P., Amaya, C., Contreras, S., Aracena, C., Pinilla, E., Altamirano, R., Vallejos, L., Pavez, J., and Maulen, J.: Oceanography time series reveals annual asynchrony input between oceanic and estuarine waters in Patagonian fjords, Science of The Total Environment, 798, 149241, https://doi.org/10.1016/j.scitotenv.2021.149241, 2021.

Pinilla, E., Soto, G., Soto-Riquelme, C., Venegas, O., and Salas, P.: Determinación de las escalas de intercambio de agua en fiordos y canales de la Patagonia, Etapa II (Región de Aysén), 2019.

Pinilla, E., Castillo, M. I., Pérez-Santos, I., Venegas, O., and Valle-Levinson, A.: Water age variability in a Patagonian fjord, Journal of Marine Systems, 210, 103376, https://doi.org/10.1016/j.jmarsys.2020.103376, 2020.

Pinilla, E., Soto, G., Soto-Riquelme, C., Venegas, O., Salas, P., and Cortés, J.: Determinación de las escalas de intercambio de agua en fiordos y canales de la región de Los Lagos y región de Aysén, Subsecretaría de Economía y Empresas de Menor Tamaño, https://doi.org/10.13140/RG.2.2.17813.65762, 2021.

Pontoppidan, M., De Falco, C., Mooney, P. A., Nummelin, A., and Tjiputra, J.: Added value of a regional coupled model: the case study for marine heatwaves in the Caribbean, Clim Dyn, 61, 3569–3579, https://doi.org/10.1007/s00382-023-06758-y, 2023.

Pujol, C., Pérez-Santos, I., Barth, A., and Alvera-Azcárate, A.: Marine Heatwaves Offshore Central and South Chile: Understanding Forcing Mechanisms During the Years 2016-2017, Front. Mar. Sci., 9, 800325, https://doi.org/10.3389/fmars.2022.800325, 2022.

Saldías, G. S., Hernández, W., Lara, C., Muñoz, R., Rojas, C., Vásquez, S., Pérez-Santos, I., and Soto-Mardones, L.: Seasonal Variability of SST Fronts in the Inner Sea of Chiloé and Its Adjacent Coastal Ocean, Northern Patagonia, Remote Sensing, 13, 181, https://doi.org/10.3390/rs13020181, 2021.

Schlegel, R. W., Darmaraki, S., Benthuysen, J. A., Filbee-Dexter, K., and Oliver, E. C. J.: Marine cold-spells, Progress in Oceanography, 198, 102684, https://doi.org/10.1016/j.pocean.2021.102684, 2021.

Schneider, W., Pérez-Santos, I., Ross, L., Bravo, L., Seguel, R., and Hernández, F.: On the hydrography of Puyuhuapi Channel, Chilean Patagonia, Progress in Oceanography, 129, 8–18, https://doi.org/10.1016/j.pocean.2014.03.007, 2014.

Shi, J., Chen, Z., Ding, S., and Lu, Y.: A Hot Blob Eastward of New Zealand in December 2019, Atmosphere, 11, 1267, https://doi.org/10.3390/atmos11121267, 2020.

Shunk, N. P., Mazzini, P. L. F., and Walter, R. K.: Impacts of Marine Heatwaves on Subsurface Temperatures and Dissolved Oxygen in the Chesapeake Bay, JGR Oceans, 129, e2023JC020338, https://doi.org/10.1029/2023JC020338, 2024.

Skogseth, R., Olivier, L. L. A., Nilsen, F., Falck, E., Fraser, N., Tverberg, V., Ledang, A. B., Vader, A., Jonassen, M. O., Søreide, J., Cottier, F., Berge, J., Ivanov, B. V., and Falk-Petersen, S.: Variability and decadal trends in the Isfjorden (Svalbard) ocean climate and circulation – An indicator for climate change in the European Arctic, Progress in Oceanography, 187, 102394, https://doi.org/10.1016/j.pocean.2020.102394, 2020.

Smith, K. E., Burrows, M. T., Hobday, A. J., Sen Gupta, A., Moore, P. J., Thomsen, M., Wernberg, T., and Smale, D. A.: Socioeconomic impacts of marine heatwaves: Global issues and opportunities, Science, 374, eabj3593, https://doi.org/10.1126/science.abj3593, 2021.

Smith, K. E., Burrows, M. T., Hobday, A. J., King, N. G., Moore, P. J., Sen Gupta, A., Thomsen, M. S., Wernberg, T., and Smale, D. A.: Biological Impacts of Marine Heatwaves, Annu. Rev. Mar. Sci., 15, 119–145, https://doi.org/10.1146/annurev-marine-032122-121437, 2023.

Soares, M. O., Rabelo, E. F., and Gurgel, A. L.: Marine heatwaves lead to bleaching and mass mortality in a key zoantharian, Mar. Biodivers., 53, 11, https://doi.org/10.1007/s12526-022-01319-8, 2023.

Soto-Riquelme, C., Pinilla, E., and Ross, L.: Wind influence on residual circulation in Patagonian channels and fjords, Continental Shelf Research, 254, 104905, https://doi.org/10.1016/j.csr.2022.104905, 2023.

Su, Z., Pilo, G. S., Corney, S., Holbrook, N. J., Mori, M., and Ziegler, P.: Characterizing Marine Heatwaves in the Kerguelen Plateau Region, Front. Mar. Sci., 7, 531297, https://doi.org/10.3389/fmars.2020.531297, 2021.

Szeligowska, M., Trudnowska, E., Boehnke, R., Dąbrowska, A. M., Wiktor, J. M., Sagan, S., and Błachowiak-Samołyk, K.: Spatial Patterns of Particles and Plankton in the Warming Arctic Fjord (Isfjorden, West Spitsbergen) in Seven Consecutive Mid-Summers (2013–2019), Front. Mar. Sci., 7, 584, https://doi.org/10.3389/fmars.2020.00584, 2020.

Takagi, S., Kuroda, H., Hasegawa, N., Watanabe, T., Unuma, T., Taniuchi, Y., Yokota, T., Izumida, D., Nakagawa, T., Kurokawa, T., and Azumaya, T.: Controlling factors of large-scale harmful algal blooms with Karenia selliformis after record-breaking marine heatwaves, Front. Mar. Sci., 9, 939393, https://doi.org/10.3389/fmars.2022.939393, 2022.

Troupin, C., Machín, F., Ouberdous, M., Sirjacobs, D., Barth, A., and Beckers, J. -M.: High-resolution climatology of the northeast Atlantic using Data-Interpolating Variational Analysis (Diva), J. Geophys. Res., 115, 2009JC005512, https://doi.org/10.1029/2009JC005512, 2010.

Wang, D., Xu, T., Fang, G., Jiang, S., Wang, G., Wei, Z., and Wang, Y.: Characteristics of Marine Heatwaves in the Japan/East Sea, Remote Sensing, 14, 936, https://doi.org/10.3390/rs14040936, 2022.

Wang, Y. and Zhou, Y.: Seasonal dynamics of global marine heatwaves over the last four decades, Front. Mar. Sci., 11, 1406416, https://doi.org/10.3389/fmars.2024.1406416, 2024.

Xie, M., Ji, Q., Zheng, Q., Meng, Z., Wang, Y., and Gao, M.: Spatial and Temporal Characteristics and Mechanisms of Marine Heatwaves in the Changjiang River Estuary and Its Surrounding Coastal Regions, JMSE, 12, 653, https://doi.org/10.3390/jmse12040653, 2024.

Yao, Y., Wang, C., and Fu, Y.: Global Marine Heatwaves and Cold-Spells in Present Climate to Future Projections, Earth's Future, 10, e2022EF002787, https://doi.org/10.1029/2022EF002787, 2022.

https://doi.org/10.5194/egusphere-2025-1421
Preprint. Discussion started: 3 April 2025

Zhao, Z. and Marin, M.: A MATLAB toolbox to detect and analyze marine heatwaves, JOSS, 4, 1124, https://doi.org/10.21105/joss.01124, 2019.